

# Initial Results From the First Field Expedition of UAPx to Study Unidentified Anomalous Phenomena

M. Szydagis<sup>\*a</sup>, K. H. Knuth<sup>a</sup>, B. W. Kugielsky<sup>c</sup>, C. Levy<sup>a</sup>,  
J. D. McGowan<sup>b</sup>, M. D. Phelan<sup>d</sup>, and G. P. Voorhis, Jr.<sup>c</sup>

<sup>a</sup>*Department of Physics, University at Albany SUNY, Albany, NY USA*

<sup>b</sup>*TekSynap, Reston, VA USA*

<sup>c</sup>*UAPx, Lake Panasoffkee, FL USA*

<sup>d</sup>*iHeartMedia, New York, NY USA*

---

## Abstract

In July 2021, faculty from the UAlbany Department of Physics participated in a week-long field expedition with the organization UAPx to collect data on UAPs in Avalon, California, located on Catalina Island, and nearby. This paper reviews both the hardware and software techniques which this collaboration employed, and contains a frank discussion of the successes and failures, with a section about how to apply lessons learned to future expeditions. Both observable-light and infrared cameras were deployed, as well as sensors for other (non-EM) emissions. A pixel-subtraction method was augmented with other similarly simple methods to provide initial identification of objects in the sky and/or the sea crossing the cameras' fields of view. The first results will be presented based upon approximately one hour in total of triggered visible/night-vision-mode video and over 600 hours of untriggered (far) IR video recorded, as well as 55 hours of (background) radiation measurements. Following multiple explanatory resolutions of several ambiguities that were potentially anomalous at first, we focus on the primary remaining ambiguity captured at approximately 4am Pacific Time on Friday, July 16: a dark spot in the visible/near-IR camera possibly coincident with ionizing radiation that has thus far resisted a prosaic explanation. We conclude with quantitative suggestions for serious researchers in this still-nascent field of hard-science-based UAP studies, with an ultimate goal of identifying UAPs without confirmation bias toward either mundane or speculative conclusions.

---

\*mszydagis@albany.edu

---

## 1. Introduction: What is/are UAP(s)?

Recently, Unidentified Anomalous Phenomena *i.e.* UAP, formerly known as UFOs, have come under increasing scrutiny, with the U.S. DOD [11], the Navy, and NASA taking them seriously. For many decades, a culture of mockery, pseudo-scientific claims, and media hyperbole created a stigma that prevented the mainstream scientific community from exploring this controversial topic. Now, in addition to our own collaboration, several academic research groups are all scientifically studying this subject [56, 61, 26, 27, 64, 54]. In a collaboration with the non-profit organization UAPx [63], UAlbany faculty have begun their own serious study to determine the nature(s) of UAP.

UAP can stand for Unidentified Anomalous Phenomenon or Phenomena, although the A can also stand for Aerial/Aerospace; UAP was recently redefined by Congress as Unidentified Aerospace-Undersea Phenomena [59, p.12]. The term aerospace broadens the study of UAP to include the Earth's atmosphere and outer space; whereas the term undersea extends it to underwater and oceanic domains. The importance of the multi-medium nature of UAPs is perhaps best illustrated by the fact the successor to the UAP Task Force is the All-domain Anomaly Resolution Office (AARO) [58]. That task force was established by the Defense secretary to provide a report to Congress [38].

The term UAP refers to an object/phenomenon which cannot be immediately recognized as prosaic, *e.g.* for aerial phenomena: human-made craft or flying animals. Unidentified only means that one does not know what something is, at least initially, until additional analyses are possible. While many UAP are ultimately identifiable, some remain unidentified. It is important to note UAP is a broad classification. It is unlikely all UAP, especially those resisting classification, stem from a singular phenomenon, and identification is not a binary procedure. It depends on the desired level of descriptive detail.

There is little doubt that the majority of UAP are misidentifications, but anywhere between 4-40% remain unidentified after careful investigations [14, 10, 29, 57], depending upon the sources and quality of the reports. Despite this, there exist hard data that demonstrate unreasonably high speeds (above Mach 40-60) and accelerations (thousands of times  $g$ ) [37, 22, 40, 21, 28, 13], without corresponding sonic booms or fireballs. Such observations represent cases of interest as they support the more exotic hypotheses, requiring novel physics or at least new engineering, but more data are needed to characterize fast-moving objects and definitively rule out observational errors [32, 30].

Making an exhaustive list of all possible explanations is not feasible; the possible explanations of UAP include, but are not limited to, airplanes, helicopters, drones, balloons, satellites/ISS and other human-made craft such as para-gliders/para-sailors, and marine vessels. Fauna were already mentioned, but natural explanations can also include: clouds (especially lenticular), atmospheric optical effects, such as sun dogs, solar/lunar halos, the Fata Morgana optical illusion and other types of mirages, plus celestial bodies, such as the Moon, Venus or other planets, meteors, and comets. It is also likely many distinct phenomena are being included under the UAP umbrella, and heretofore unknown or unexplained (undiscovered) or sparsely studied atmospheric phenomena may be involved, such as ball lightning [8, 47] and/or earthquake lights [20, 49, 19]. Both of those have been considered “pseudo-scientific” [50].

It is this vast number of prosaic explanations, both known and unknown, which makes identification a major challenge. However, enough reports from serious and legitimate sources [29, 53] clearly highlight the need to study UAP scientifically, while reducing biases. Groups such as UAPx [63], IFEX [26, 27], VASCO [61], and the Galileo Project [31] are each undertaking this task now. Villarroel and her group (VASCO) have already made seminal discoveries of concrete anomalies, multiple light sources appearing and vanishing [61, 48].

### *1.1. What is UAPx?*

UAPx is a (501c3) non-profit organization co-founded by Naval veterans Gary Voorhis and Kevin Day, who were involved in the (2004) *Nimitz* carrier strike group UAP encounter [42]. One of the first organizations of its kind to collect data, it was founded at a similar time as the Galileo Project, and has similar aims. UAPx recruited scientists, engineers, and technicians to work alongside experienced military veterans, for the purpose of collecting and scientifically analyzing new data on UAP. This is distinct from reanalysis of historical UAP cases. That work is already done by multiple individuals and organizations: *e.g.* SCU (Scientific Coalition for UAP studies [23]) plus MUFON (Mutual UFO Network [36]). These existing groups diverge significantly in amount of participation by scientists/engineers and level of scientific rigor. The approach taken by UAPx ensures data quality, chain of custody, data provenance, and rigorous data analysis. Having multiple independent groups is useful for cross-checking claims, as in particle physics and other fields.

Scientists collaborating with UAPx constitute a wide range of differing expertise and informed opinions; they strive for an introspective self-skepticism, aiming for the difficult balance between openness to speculative ideas on the

one hand, versus “debunking” on the other, aimed exclusively at explaining all ambiguities as part of known phenomena only, regardless of context.

### 1.2. *The Objectives of UAPx*

UAPx is devoted to identification and classification of the initially unidentified and unclassified. While open to the techno-signatures possibility, as astronomers should be [60], including near-Earth signatures, it doesn’t exclude mundane options nor prefer speculative ones, respecting Sagan’s dictum regarding extraordinary claims and evidence, but not blindly. Its main goals:

- Acquire data which fill the gap in the scientific knowledge of UAP due to a lack of high-quality, unclassified data.
- Make said data as well as analysis results publicly available. Data and results will be released only after analyses are completed. Completion is defined as peer-reviewed publications in scientific journals.
- Combine existing hardware in new ways as well as develop new sensors as needed, in order to accomplish the first two goals.

In service of all three of these objectives, UAPx has developed, and continues to refine, methods for the collection of quality data on UAP, through the use of a small-scale (portable, table-top, lightweight), but diverse and advanced, multi-spectral suite of sensors, covering not only the EM spectrum, but also E/B-fields [35], ionizing radiation, and other types of measurements, made robust by calibrations before, during, and after field deployments [56].

## 2. Methodology

Watters *et al.* [64] describe the challenges faced in UAP studies in great detail, explaining how and why we can build on “gray” literature (non-science publications) including anecdotal evidence, for sensor choice. They establish global objectives for this kind of science, and provide a framework and a road map for discoveries. While this publication came after we already started our endeavor, it provides a foundation to build upon (so that it is unnecessary to dwell on the fundamentals of the scientific method and proper analysis here). It already addresses the needs for control and background data, bias mitigation, some form of reproducibility, and inclusion of statistical and systematic uncertainties. Together with moving away from reliance upon eyewitness testimony, these tools should help move the study of UAP out of the “fringe.”

UAPx uses a diverse set of sensing devices, in order to capture different types of data on several channels. The collaboration’s strategy involves:

1. Commissioning multiple cameras and multiple copies of other sensors, to capture the same phenomenon from different angles, at high resolution, for robust estimation of distance, size, speed, and acceleration by triangulation made possible by precise instrument locations [51].
2. Coincidence timing across all devices to help in a faster data reduction resulting in lists of ambiguities and true “anomalies.”
3. Eventual construction of (semi-)permanent stations using automated, remote sensor suites, to serve as (near-continuous) data collection stations, in both control areas as well as supposed UAP hot-spots.
4. Corroboration of anomalies via use of public sources of data, including but not limited to Doppler weather radar data, any unclassified satellite imagery, as well as global particle/radiation detection networks.

To serve points (2) and (4), Monte Carlo simulations and both Bayesian and frequentist inference will be applied to determine the probability of two or more events overlapping in time being due to accidental coincidence. AI/ML (Artificial Intelligence / Machine Learning) will also play an instrumental role in UAPx, for a non-binary and multi-stage classification, beginning with motion detection, for infrared (IR) and for visible light. In the first expedition (Section 4), (1) was only partially successful, as only one non-IR camera was permanently running, (2) was hampered by imprecise timing, to be discussed later as a lesson learned, (3) is a longer-term aim, and (4) is underway.

### 3. Instrumentation

#### 3.1. Visible Light Imagery (UFODAP)

For visible and near-IR (night-vision mode for lower-light conditions) imagery, UAPx selected, for its first expedition, the UFODAP (UFO Data Acquisition Project) [39]. The UFODAP was chosen due to its (advertised) ease of use, data security, and an optional collection of secondary sensors: magnetometer, GPS, 3D accelerometer, and built-in ADS-B for flight tracking. The Dahua 50232 PTZ (pan-tilt-zoom) camera, capable of physically tracking potential objects of interest through the UFODAP’s OTDAU (Optical Tracking Data Acquisition Unit) software, used a commercial machine vision algorithm to identify moving targets and track them by rotation of the camera lens as needed. It was tuned to its default high sensitivity for the July 2021 Catalina mission, to avoiding missing any potential anomalies. (One example of a potential UFODAP alternative is Sky360 [24], formerly called SkyHub.)

A 1/2.8-in. 2 MP STARVIS CMOS Sensor provided 20-30 fps at 1080p resolution (max) with a  $125.6^\circ$  (horizontal) by  $73.4^\circ$  (vertical) field of view. The proprietary “Starlight” technology for ultra-low light sensitivity could capture details in low-light conditions down to 0.005 lux, resulting in reasonable images even for dark environments like a night sky. Depending on the focal length set, between 4.9-156.0 mm, the resolution in arcseconds was 120-3.83. The maximum possible (optical) zoom went to 32x.

An optional add-on is a fisheye camera (model DH-IPC-EBW81230) with a nearly complete view of the sky. Without its presence, the PTZ camera can self-trigger instead of being triggered by the fisheye. While the disadvantage is a smaller number of pixels for the same event, if it can identify a positive target through the OTDAU software it can instruct the PTZ to lock on and track a target. One or both cameras can be mounted to the top of a vehicle for increased mobility, and in our case the fisheye was permanently mounted in this fashion, not coupled to the PTZ. The vehicle used by UAPx was the O.S.I.R.I.S. [25] (Off-road Scientific Investigation and Response Informatics System) and its purpose was a rapid deployment for providing an additional, mobile vantage point to aid in triangulation.

The UFODAP system does not record without a trigger, so it does not overwhelm storage capacity with non-stop, high-quality video. However, this comes with a downside: if the trigger isn’t well calibrated and set up, only a few frames may be captured for ambiguous events. That makes them difficult to analyze, especially for objects or events not expected or difficult to detect by the OTDAU software, as may be the case for classic UAP.

Between 22:35 Pacific Sunday July 11 and 12:40 on Friday July 16, 2021, 1716 AVI files were saved from the UFODAP, with the majority  $O(1)$  second in length or even shorter (a few frames in many cases). Because of meta-data blocking portions of frames, two versions of each of the 1716 files exist, both with and without reticles, date, temperature, angle, and other information, for the purposes of having both unobstructed views, plus all of the relevant meta-data.

The top row of Figure 1 shows the physical system from different angles and in different contexts. The bottom row shows two sample images, of the same field of view, at the default orientation, prior to any PTZ rotations, at different times of day. The observation point was within Laguna Beach, CA with the field of view centered on an azimuth of  $260.5^\circ$ , providing a view of Catalina Island across the channel. The lower right has a single video frame from the most perplexing ambiguity captured during UAPx’s first expedition.

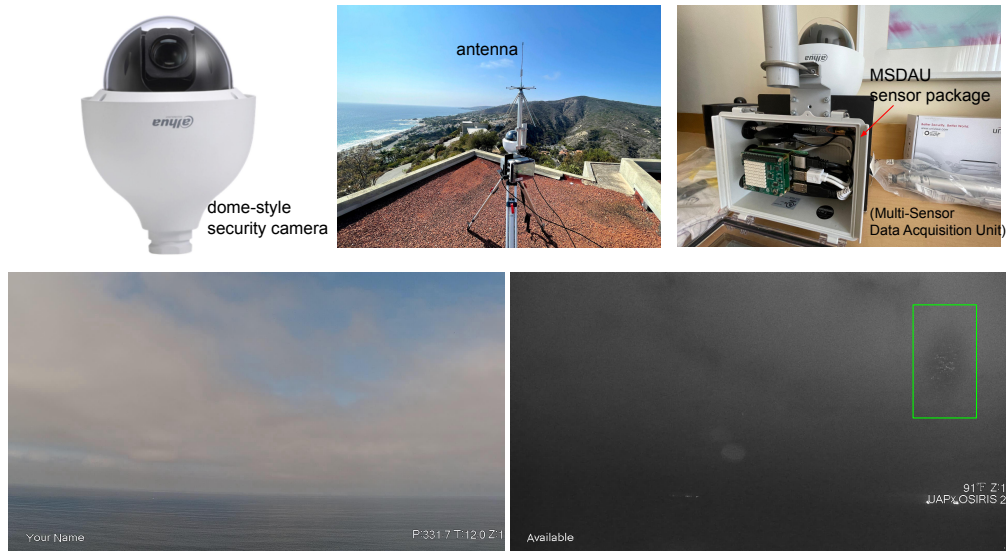


Figure 1: Upper left: Example Dahua 50232 camera at the heart of the default UFODAP system. Upper middle: A UFODAP unit deployed on a roof in Laguna Beach, California in mid-July, 2021. (The discone antenna is for RF spectrum analysis, but it was uncalibrated and has not yet been used by UAPx.) Upper right: A sensor package that came with the UFODAP for UAPx, with the cover removed to display the internals. Its software was not functional during the first field expedition, but sensor data will be recorded in the future. Bottom left: An example daytime UFODAP image of the Catalina channel, at 1920x1080 resolution. Bottom right: The view from the same perspective but at 4am. In this sample, a dark spot of unknown origin with bright pixel clusters within is present (green box).

### 3.2. IR: Night Vision and FLIR

The utility of infrared videography has been demonstrated by the *Nimitz*, *Roosevelt*, and other U.S. military (Navy) incidents. Not only does IR videography provide the ability to capture images at night, but it also provides data on the temperatures within the field of view, and can reveal the presence, or absence, of high-temperature exhaust. That said, for all of the IR equipment we only possessed the existing internal calibrations, and thus our devices were more useful for measurements of relative not absolute temperatures (simply cold vs. hot), and for contrast against the background.

UAPx employed several pairs of AN/PVS-7x night-vision goggles, useful for manual spotting, as one could not record (directly). Smartphone cameras held up to the night-vision goggles did provide an elementary recording capability for potentially interesting events (example in Figure 2, now explained).

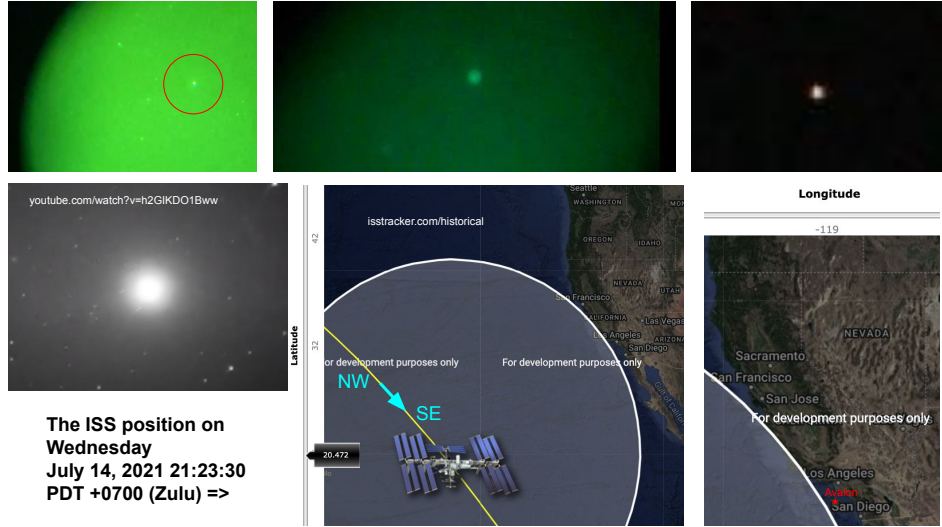


Figure 2: Upper left: A video frame ( $720 \times 1280$ ) showing a spheroid in night vision (phone recording). It neither blinked nor made noise, but was later identified as the ISS. Upper middle: An example from another phone ( $480 \times 640$ ) that captured the same object, concurrently. Upper right: A movie camera belonging to the documentary crew also recorded it. Bottom left: Online example of the ISS in night vision, for a qualitative comparison. Bottom right: Details on the ISS location at the time (site used in beta-test mode). The white curve denotes the edge of a nominal 50-mi.-radius horizon, but Avalon on the island (where the videos were shot) could still see the ISS for  $\sim 120$  s due to altitude and weather.

The primary imaging systems used on the expedition were 8 FLIR ThermoCam PM695 units. These were deployed on the mainland (Laguna Beach) on the same flat roof as the UFODAP unit discussed in the previous section, and pointed in the direction of the Catalina channel. They were oriented with slightly overlapping fields of view, to allow for triangulation – although with large uncertainties due to the units’ proximity to one another. They recorded imagery using a  $720 \times 360$  uncooled microbolometer array with spectral sensitivity from  $7.5\text{--}13 \mu\text{m}$  and field of view of  $48^\circ \times 36^\circ$ . The units were operated at 60 fps and the resolution was up-scaled in software to save files as  $1440 \times 720$  MP4s with two 4-channel AJA Ki-Pro-Go digital video recorders. Via FFmpeg [12] as the first step, videos were analyzed frame by frame, at the higher resolution, with human-eye quality assurance on motion detection of discrete pixel clusters moving across the screen combined with threshold variations. The image frames were cropped to address (bouncing) cursor misbehaviors. (The FLIR cameras were deployed near Seattle before this study for years.)



### 3.2.1. C-TAP FLIR Image Analysis

A new software package was developed by Szydagis for rapid image processing of FLIR recordings which has been dubbed C-TAP (Custom Target Analysis Protocol), capable of detecting discrete objects traversing a screen, even in conditions of rolling clouds, by means of a naïve Bayesian classifier applied primarily to the minimum and maximum differences in pixels between frames, and the standard deviation across RGB pixel values, for helping differentiate (physical) objects captured crossing the fields of view from camera noise. Only color-mapped RGB values were available, not mono-channel intensity data from the microbolometers within the PM695s. This suggests the ability to distinguish noise using the RGB standard deviations was an effect from the internal software the PM695 uses to render temperature colors.

To cross-check C-TAP, developed for FLIR, against the UFODAP algorithms for a “regular” camera, C-TAP was also applied to the 1716 UFODAP videos. It found  $\geq 1$  valid triggers using its own logic in 85% of the videos.

The C-TAP procedure consists of pixel-by-pixel subtraction of each frame from the preceding frame, similar to what has been done for bubble chamber imagery from direct dark matter searches [52]. One single background image for subtraction could not be generated, as the lighting and weather conditions were constantly changing. Furthermore, one of the goals was to capture craft in motion, making it necessary to default to using only the preceding frame for comparison. This method is sensitive to objects either hotter/colder than their environment. Either object type causes both negative and positive values in subtraction, alternating, during a crossing of the field of view of one of the cameras. The best processing time of  $\sim 1.5:1h$  was achieved with GPUs.

After calculating the average in the pixel differences across an entire hour for each of the FLIRs, C-TAP sets a threshold  $3-5\sigma$  above this floor, unique to each video. It is adjusted depending on the nature of the noise, such as a severe non-Gaussian upward tail, typical of the older (noisier) camera units, necessitating setting a threshold toward the upper end of this range to avoid a high false-positive rate. A difference was discovered between camera noise and what appeared to be real/physical, moving objects based on the standard deviation  $\sigma_a$  in six values: the greatest pixel differences in RGB, positive and negative.  $M = \max(|p_f - p_i|)$ , where  $p$  denotes an 8-bit (0-255) pixel value, and  $M$  denotes the maximum negative difference (*i.e.*, the minimum) or the maximum positive difference. A lowercase or an uppercase subscript indicates minimum or maximum, respectively. The relevant equations follow:

$$\sigma_a = \sqrt{\Delta R^2 + \Delta G^2 + \Delta B^2 + \Delta r^2 + \Delta g^2 + \Delta b^2} \quad (1)$$

$$\text{where } e.g. \quad (2)$$

$$\Delta R = M_R - \mu_a \text{ and } \Delta r = M_r - \mu_a \quad (3)$$

$$\text{and similarly for G, g, B, and b. The mean is defined as} \quad (4)$$

$$\mu_a = (M_R + M_G + M_B + M_r + M_g + M_b)/6 \quad (5)$$

Noise tends to increase or decrease the pixel values together across the 3 color values red, green, and blue, leading to a smaller  $\sigma_a$ . Meanwhile, true external events tended to have a greater value (Figure 3). As microbolometers simply detect IR photons, yielding only one measurement (of intensities), this again implies glitches existing in the internal false-color-rendering software.

In order to determine which imagery seemed the result of physical events external to the camera, for effectively defining a control data set for C-TAP training, initial C-TAP post-processing triggers resulting from either single-pixel or single-frame anomalies were rejected as false. Furthermore, volunteer video reviewers would (slowly and fully) watch videos to look out for discrete clusters of pixels traversing the screen, in two or more frames, taking either a linear or curved path. Different individuals would review the same videos as a cross-check, to reduce human bias. C-TAP parameter values for the different steps of its processes summarized here would be updated until an optimum balance was found, maximizing the acceptance of events which appeared to be legitimate while minimizing the acceptance of those which appeared to be background noise only, with no clear object in view.

The process of human validation for tuning C-TAP results was iterative. A team member would view an entire video, making a list of frames of possible interest. Both the same and a different teammate would verify C-TAP agreed on these frames. Both would go back to confirm the objects caught by C-TAP but not by eye originally were visible, with the individuals involved logging both false positives as well as false negatives, clear objects (any kind) missed. C-TAP settings would be adjusted to reduce both types of events. To reduce fatigue, the videos would be shortened with each viewing to only frames still deemed of interest. On average, this method tripled the number of detections.

Classification of objects deemed legitimate by the combination of human quality assurance and automation will be a 2nd C-TAP module. Wing flapping for birds and FAA records for planes, *e.g.*, can determine the truth for training. After it is complete, C-TAP will be made open source (on GitHub).

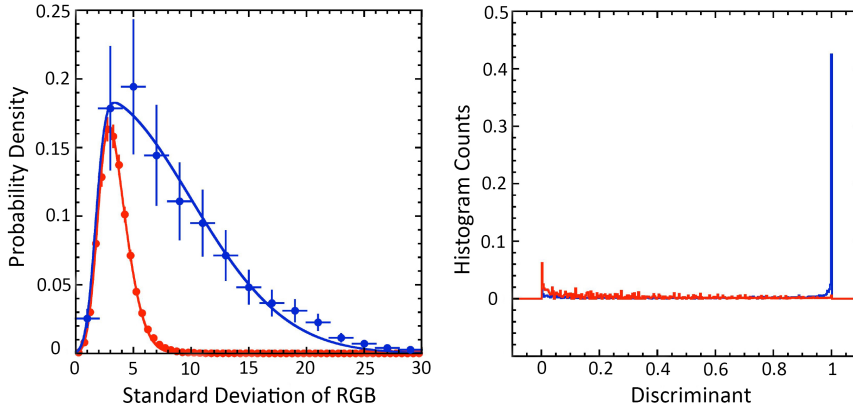


Figure 3: Left: Histograms of the standard deviations  $\sigma_a$  from “good” (signal) and “bad” (background) events in blue and red, respectively, with skew-Gaussian fits to each. The y errors are  $\sqrt{N}$ , based on the number of events in each bin, while x errors are bin widths. One sample hour of FLIR video data was used, chosen for its mixture of clear and cloudy conditions and lighter mixed with darker conditions (dusk), and medium camera quality. This plot is a final asymptotic result from many iterations of human-eye scans at different thresholds to separate signal from backgrounds. Right: The classification-score output of a naïve Bayesian classifier based upon the skew Gaussians at left, for separating signal from backgrounds. 0.5 was the default value for separation (as is common for neural networks).

### 3.3. Radiation Detection

Some documented UAP encounters involve apparent harm from ionizing radiation, *e.g.* the Cash-Landrum [46] and Rendlesham Forest [41] incidents. One of the benefits of working with radiation detection is that it is typically easier to analyze compared to images, as radiation detection can be as simple as lists of times and energies. As far as what is knowable from public sources, there are also no known air- or spacecraft in current operation that produce measurable quantities of radiation, at least not at large distances.

Terrestrial and cosmic sources exist and vary in intensity by location, so a coincidence measurement, combining radiation sensing with *e.g.* a camera ambiguity, is key for identifying potential multi-channel events of interest. An event superficially anomalous in terms of its energy may be a solar or galactic cosmic ray, or be extra-galactic, originating from a distant supermassive black hole or a supernova. Cosmic rays have been measured beyond  $10^{14}$  MeV [1], and gammas  $> 10^8$  MeV, traced in the latter case to the Crab pulsar [2]. The higher the energy the lower the flux, so the lower the probability of detection.

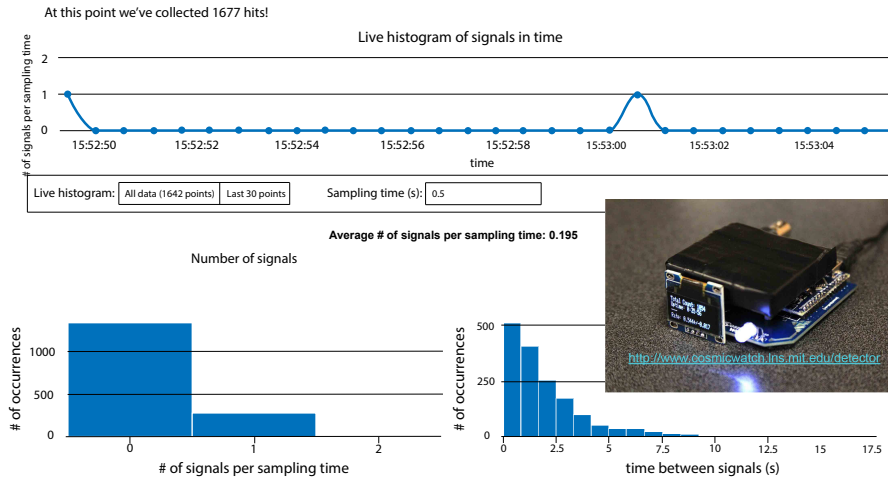


Figure 4: Screenshot of the live Cosmic Watch software (site). Inset: Unit without a cover.

UAPx uses the Cosmic Watch developed by MIT [6, 4], intended primarily for muon detection, but capable of detecting various different interaction types (although without particle ID or direction). The Cosmic Watch has the advantage of measuring both count rate and energy, not simply the former as in the case of the older Geiger-Müller counter. It is also smaller and trivial to deploy, coming with existing software (Figure 4) for USB data taking. The device itself consists of  $5 \times 5 \times 1$  cm of plastic scintillator instrumented with a SiPM (silicon photo-multiplier) operated by an Arduino Nano (Figure 4, inset). Every unit constructed will have variations in threshold and efficiency, leading to distinctive default rates. The exact unit used at Laguna Beach, CA was calibrated both by just measuring the ambient radiation environment at UAlbany SUNY over the course of the year preceding the expedition, as well as with multiple alpha, beta, gamma, and neutron sources to ensure robust energy reconstruction ( $dE/dx$ , not energy, for non-stopped particles).

While the source calibrations were focused on deposited energy, the rate of cosmic rays is well known as a function of both the altitude and latitude and well studied utilizing Cosmic Watches [5]. Particle flux will increase with the former (up to a point) with less atmosphere for particles to traverse, and also increase with the latter, closer to the geomagnetic poles (due to the charged-particle component). A count rate vs. energy for UAlbany (compared to the spectrum from UAPx's first expedition) can be located in Section 5. Unique, newer units purchased after the expedition have had additional calibrations through cross-country drives, airplane trips, and underground lab visits.

### 3.4. Future Instruments: Ultraviolet, Electromagnetic, and Piezoelectric

We next briefly describe instrumentation planned for use on future investigations, beginning with sensitivity to a broader range of photon wavelengths. To supplement our visible-light, low-light / near-IR, and FLIR (far-IR) cameras, we will add UV imaging, used previously by atmospheric scientists for photographing lightning in slow motion. This is an unexplored new realm for UAP research; this is motivated by claims of Doppler blue-shift of observable light. Moreover, improved FLIR cameras have been secured, light models usable by smartphone. Claims exist of anomalous objects in the sky, observable in one wavelength range but not in another (*e.g.*, only IR-detectable [54] or in visible light only) so these observational capabilities could bear important fruit, for unknown natural phenomena and/or for signature management.

Many reports connect UAP with electromagnetic effects, such as vehicle disruption and deactivation, and other (electronic) equipment failures [7, 16, 45, 33]. So, in addition to capitalizing upon the magnetometer inside of the UFODAP, we will employ robust off-the-shelf 3D EMF, or “trifield,” meters, along with smartphone magnetometer apps that use a phone’s existing hardware. These have the advantages of low cost, portability, and ease of usage. A quick calibration of one (Appreciate Studios), moving the phone running the app away from a strong (rare-earth) magnet in discrete steps along a ruler, yielded a power-law exponent of  $-2.74 \pm 0.09$  for the magnitude of the measured B-field as a function of distance, not far removed from the theoretical value of -3 for a perfect dipole. For future expeditions, a magnetic gradiometer is also under construction at UAlbany SUNY. The planned gradiometer will be far more powerful, able to detect metal like that in a passing car from up to 30 meters away.

Lastly, piezo-electric acoustic sensors will be used to seek anomalies from the infrasound to ultrasound ranges, which could be caused by air disruption due to hypersonic travel [34]. Infrasound may also induce hallucinations, so it is a plausible explanation for the more unusual UAP-eyewitness claims [18]. UAlbany owns piezos previously useful for (dark-matter-seeking) superheated droplet detectors, though these listened mainly for ultrasound [3]. UAPx has also attempted to access data from existing global infrasound networks used to ensure compliance with nuclear test-ban treaties, though without success. As always, to confirm if any ambiguous findings can robustly be claimed to be anomalies, coincidence windows with other sensors will remain key, especially since calibration and background characterization in a noisy environment will be challenging (ground, sea, or sky) even given frequency analysis (FFT).

## 4. Laguna/Catalina Expedition

### 4.1. Context and Equipment List

From July 10-17 of 2021, UAPx conducted an expedition with two locations, a flat rooftop in Laguna Beach, CA, and another in Avalon on Catalina Island, which was a purported UAP hot-spot prior to the *Nimitz* event [42]. (The timing reduced the probability of a fully cloudy week.) A third but moving viewpoint was provided by the O.S.I.R.I.S. As delineated in the previous sections, the team deployed 1 UFODAP with a PTZ and a fisheye camera (although the fisheye was separate and used solely on the O.S.I.R.I.S.' roof), two pairs of night vision goggles for use by the island team, 8 FLIR cameras, and 1 Cosmic Watch. (Other tools were less useful, and so they are not listed.)

### 4.2. What was Successful and Unsuccessful

While several observations were at least initially intriguing, the primary purpose of the initial outing, in retrospect, was effective field testing of all the equipment and analysis techniques. Lessons learned include the following:

- The UFODAP hardware should be of sufficiently high quality to serve as scientific instrumentation, but its software is not reliable for object tracking and identification, nor is the software capable of accessing the MSDAU (Multi-Sensor Data Acquisition Unit), the name given to the non-optical sensor collection, and as a result no ancillary data, such as GPS location and ADS-B exchange, were recorded.
- Tracking just aircraft, via transponders, is not sufficient. It is also necessary to have apps showing maps of satellites (especially Starlink, often mistaken for UAP), all known rocket launches, and the ISS' trajectory. (See Section 5.2 for a more quantitative study of our ISS observation)
- Multiple identical cameras are still a necessity, even if others can supplement the UFODAP like FLIR. All must have battery backups.
- Having many FLIR cameras was not as beneficial as originally expected. They generated a large amount of data that wasn't of the highest quality, and challenging to analyze in a reasonable time given limited manpower/CPU's. Instead, fewer, more modern, and better calibrated units would be optimal. If lightweight, they can then be slewed on a gimbal to point in the same direction as the UFODAP, when it rotates to follow an object. Angular information can be transmitted using software. All connectors must be RF-shielded (with metal) against stray EM noise.

- All clocks must be synchronized, ideally at the sub-sec. level, and device positions recorded using a combination of GPS with a laser range finder. Working with a film crew, necessary for our seed funding, created distractions that led to these and other critical steps being neglected.

Lastly, more than two Cosmic Watches running in coincidence mode allow for a reduced background rate as well as rudimentary directionality. Alternatively, separation of a pair outside the typical diameter of cosmic-ray showers results in a greatly reduced background, permitting any anomalies to be more obvious. It is important to note, however, that due to secondary particle production from GeV+ muons, shielding increases the background rate.

## 5. Example Observations and Preliminary Results

### 5.1. UFODAP: Its Titular Ambiguity

The UFODAP system ultimately made a detection that remains the expedition’s most intriguing ambiguity. Multiple camera ambiguities (multiple videos close in time on the minute scale) were not discovered in a systematic review of the recordings by person or software. These ambiguities appear associated, at least temporally, with the highest-energy event measured in the Cosmic Watch, by itself not necessarily anomalous, as explained in Section 3.3, and further explored in 5.4. This is a timeline (in PDT) for Fri. 07/16/21:

- 3:50:14am. A “blank” video *i.e.* without an obvious trigger condition
- 3:57:16. A diffuse dark spot appears at upper right. Its appearance may have triggered the UFODAP. It has no well-defined edges (Figure 5).
- 3:57:27. The spot remains; the camera slews, chasing an insect separate from it. During rotation, white dots that turn into black streaks appear, emanating from this spot. Note that the spot is not visible in the later frames where the background sky is well-illuminated. (Fig. 6, 20 fps)
- 3:59:24. The camera is again stationary and the dots are visible within the spot for the entire video’s length, though the spot vanishes (lightens to match the surrounding gray cloud color) and a new white dot appears in frame 13 where the spot was located, along with a new black dot, in a different area. All frames are shown as Fig. 7 (full-res, zoomable) and 8. The transient nature of our dots is not inconsistent with [61, 48], and they may be part of a significant larger background of objects [62].
- 04:00:13am. The first “normal” video after the incident. This video and all of those above were quite short (a few seconds each at the most).

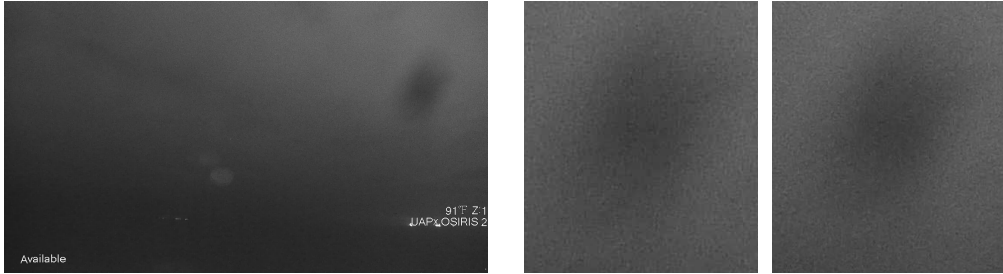


Figure 5: Left: The 3:57:16am spot, at upper right, in the first frame of the video. Middle: A zoom in from that frame. Right: A zoom in from the final frame. No obvious changes occurred in the spot or anywhere in the field of view. (No white dots were evident yet.)

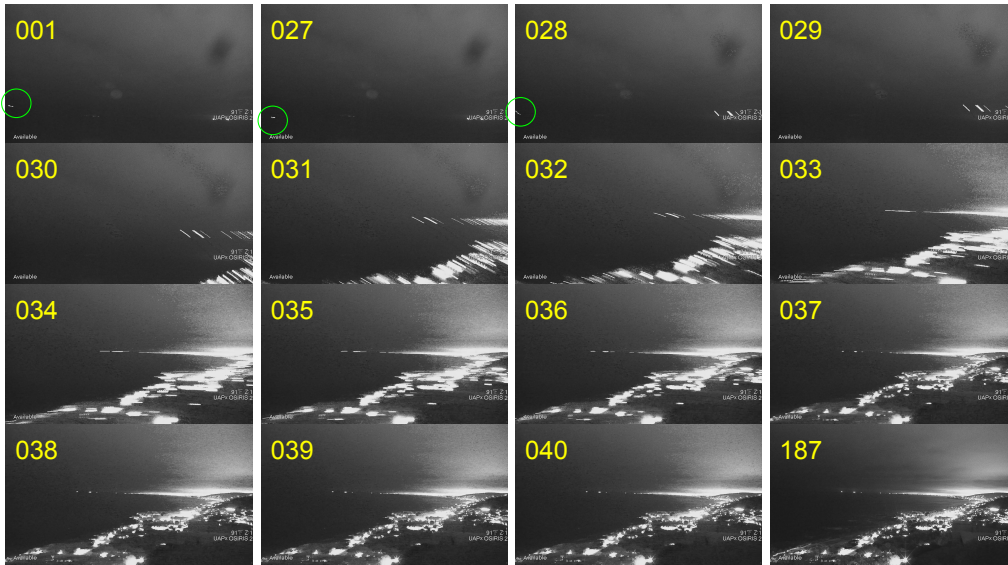


Figure 6: Selected images from the 187 frames of the 3:57:27am video, identified by frame number in yellow at upper left in each image. An insect unrelated to the dark spot (in green circles, first three images) appears to be the catalyst for the camera rotation which begins with frame 28; it is illuminated by porch lights from below. (Frames 2-26 are omitted due to their near-identical, nearly static nature, as well as #s 41-186.) The dark spot from the previous video, depicted in Figure 5, remains at upper right. During the lens' motion, the spot does not appear to move, at least initially. This lack of apparent motion could be due to its diffuse nature, or this could suggest it is a lens artifact, not a water droplet or a fly, especially since the spot is not at all visible in the later frames in which the sky is better illuminated. Another possibility is parallax due *e.g.* to a faraway atmospheric effect. The white dots within the dark spot first start to appear in frame 28, then appear to streak as if real, along with the city lights at lower right, although their streaks are black, not white. These dots start to merge with obvious noise (qualitatively similar to them) in frame 32.



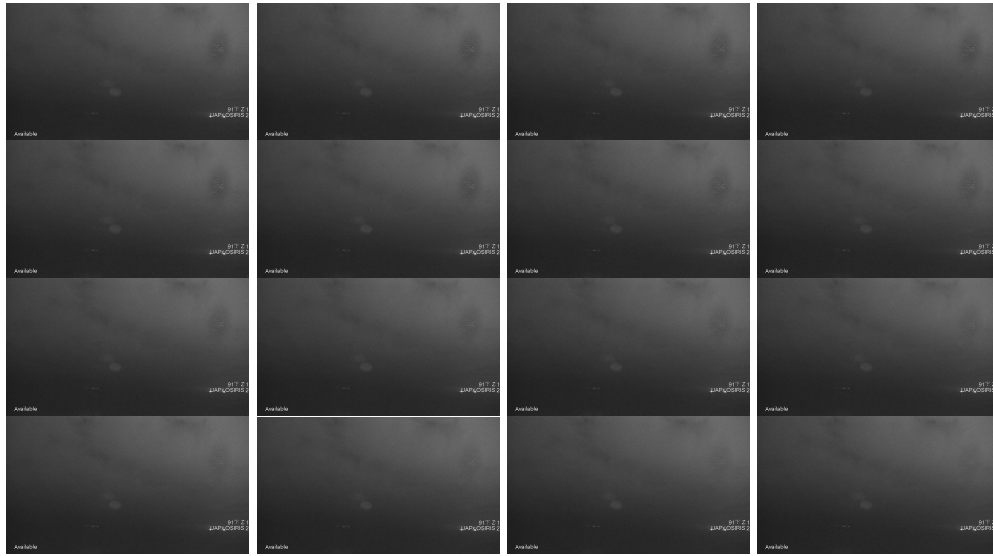


Figure 7: All frames of the 3:59:24am video; temporal progression is left to right then down, with 0.050 s in between. (This video and all others will be made available, uncompressed.) The disadvantage of an uncalibrated, triggered system is: no images immediately preceding and succeeding these frames are available, so it is impossible to see the immediate origins of the spot and dots, or their departure. Continuous recording is the plan for the future.

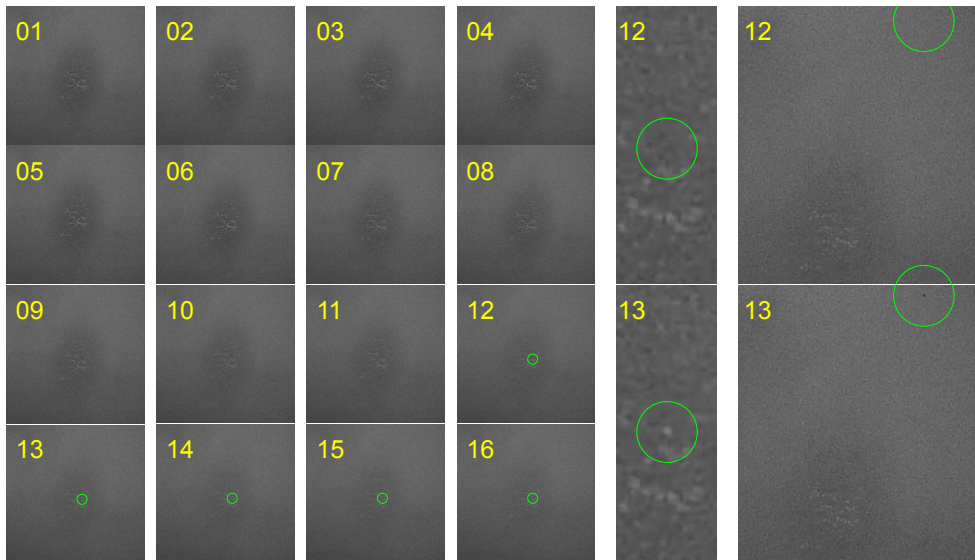


Figure 8: Left: Zoom-in on the dark spot from Figure 7 with green circles indicating the appearance of a new white dot between frames 12 and 13. Right: Further zoom on frames 12-13 only for greater ease of seeing the appearance, concurrent with a black dot emerging. The behavior of our dots is similar to that of historical transients discovered in [48, 61].



Figure 9: A false-color (blue) correlation map of pixel intensity behavior over the 12 (out of 16) frames of the dark spot vanishing. There exists some correlation between the behavior of the cloud cover and the behavior of the dark spot, implying it is an atmospheric effect. Its disappearance could have been due to a lower level of clouds condensing across the sky.

We evaluate ten prosaic (“null”) hypotheses put forth both inside/outside our group. Our list is an attempt at completeness, for ruling out or in, even though that is never fully practical. (However, in this case and in others, UAP cannot just “be anything,” a common phrase used in debunking.)

1. Fall-streak hole from aircraft, with the white dots the aircraft, or noise (or: natural cloud formation, Fig. 9, least improbable by elimination)
2. A star field or seagull flock producing white dots, as viewed through a hole in the clouds, the dark spot, either a natural or fall-streak hole
3. Water drop evaporating, evident as a spot slowly decreasing in area
4. Fly on the protective dome leaving, evident as a spot suddenly gone
5. Cosmic-ray shower, where ionization lights up CMOS pixel clusters
6. Meteor breaking up or meteor shower: fragments of a single meteor or multiple meteors showing up as dots, and making a hole in the clouds
7. Camera noise in the dark environment, possibly combined with a residual effect from the camera rotation earlier: white dots and streaks
8. Resetting of camera levels for a lightening sky, which should manifest as a change in pixel intensities across an entire image
9. Military testing tied to a nearby base and/or training area of operation, where the white dots are *e.g.* a drone cluster, creating a hole (1)

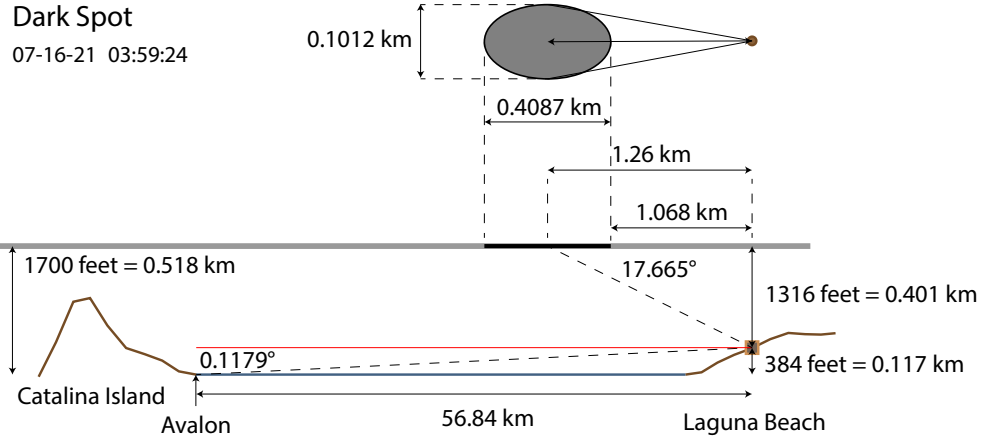


Figure 10: An illustration of the geometry of the dark spot assuming that it was a physical, elliptical hole in the clouds within the cloud ceiling at the time. If the white dots were real objects at the ceiling, they were each  $\sim 4\text{m}$  wide, applying Eq. (7) introduced later.

10. The reflection of lights in the camera dome from the nearby cities leading to white dots, inside of a water drop for instance (Hypothesis 3).

The fall-streak hole hypothesis (1) explains a dark spot, but not the white dots (bright clusters of pixels) although those are potentially explained by the camera noise hypothesis (7). This explanation (1) fails however, as no aircraft could be identified as being in the area at the time, to cause a fall-streak hole. Moreover, the atmospheric conditions were nowhere near what is required for a naturally-occurring fall-streak hole (*i.e.*, it was not sufficiently cold even at the altitude of the cloud layer for supercooled water to exist and then freeze). If this were a natural hole between clouds, then the star field hypothesis (2) would be possible, but it is not likely due to the fact the pattern of dots is too dense (considering LA's light pollution) and does not match the known local sky. The dots are too bright to be high-altitude gulls instead, and it would be improbable for them to be clustered in the hole, even accounting for flocking.

Unlike the fall-streak hole hypothesis (1), the star field or flock of seagulls hypothesis (2) cannot resolve the rapid lightening of the dark region, since the distance and size, as illustrated in Figure 10, would imply clouds moving on the order of  $100\text{ m/s}$ , although the behavior of the dark spot, correlated with that of the overcast sky (Figure 9), suggests that the spot was occluded by condensation of a lower level of humidity across the visible sky. Even if the atmospheric conditions were correct, this fails to address the dots remaining, if they are camera noise (not necessarily the case, as we address later).

The next two hypotheses involve something close to the camera instead of a physical event detected in the clouds, so they are sequential in our list. The dark spot fades away much too quickly to be water (3) evaporating naturally, especially since evaporation occurs at a liquid droplet’s surface. That means the dark spot would slowly decrease in size as evaporation occurred. This is not what happens—the spot lightens uniformly. Moreover, there was no rain at the time and the temperature was well above the dew point. The house on whose roof the UFODAP had been deployed was 120 m above sea level and too far inland (0.45 km) for sea spray to be a possibility. If this were a drop of dew, it should’ve had a mass  $\approx 50$  mg so we can estimate the power needed to evaporate this water mass at a rate matching that of the spot fading:

$$Q = mL_v = (0.05 \text{ g})(2260 \text{ J/g}) = 113 \text{ J}. P = (113 \text{ J})/(0.6 \text{ s}) = 188 \text{ W}. \quad (6)$$

Even given an order of magnitude error such sudden power is unreasonable.

The fly explanation (4) is similar, but is more plausible. However, a fly’s presence on the outer dome does not explain why the first 30 or so frames of the 3:57:27 am video (Figure 6) show the dark spot, while the later frames do not, with the spot reappearing for the 3:59:24 am video (in Figure 7). The fly hypothesis also does not explain why the behavior of the lightening dark spot is correlated with the behavior of the cloudy sky (Figure 9). Only a fly taking a specific, slow departure path could exhibit such a correlation. Additionally, the fly hypothesis requires something like camera noise (7) for the white dots, with the fly providing a dark spot, with thermal/shot noise within it.

Cosmic rays (hypothesis 5) seem even more natural, given it was a Cosmic Watch detection which led to the discovery of the videos in question and the fact CCDs are known for radiation detection via ionization. They are, in fact, employed as dark matter detectors [9]. However, the localization is not natural, especially since camera lenses are only able to focus observable light (not gamma rays nor cosmic rays, of course). A cosmic ray shower should have affected most of the field in the CMOS, not CCD in our case—not just a particular region. Moreover, the cosmic ray hypothesis doesn’t address the dark region in general, and the improbability of all of the dots to be within it.

Another explanation (6) that involves an external, astronomical origin is meteor(s). It fails as well, because no dramatic meteors were reported in the area at the time, neither one breaking up, nor a shower of multiple, and such non-streaking (static) behavior is not common, requiring a head-on view.

The noise hypothesis (7) is promising, not only for the white dots, but the dark spot itself, as the latter’s darkness (still requiring its own explanation)

may have caused the former, but this type of noise was only observed during lens motion, never in stationary cases, like Figures 7-8. All of the crew were asleep at the time and accounted for, so it is not possible that a team member walked by and inadvertently shook the system at the time. Most importantly, the brightness of the white pixels is not Poisson-distributed, as for examples of camera noise that appear superficially (visually) to be the same (Table 1).

	Case A	Case B	Case C	Case D
$\mu$	82	89	65	66
$\sigma^2$	51	98	21	40

Table 1: The means and variances of sets of 8-bit pixel values. Case A is the dark spot, B is the same area but within an image without the spot, C is a control area from the same image as A, and D is for the same control area as B for an image without the dark spot.

The table shows the variance was 51 for a mean of 82, as reported on a black-and-white scale of 0-255. This is sub-Poissonian by nearly 40%. For a Poisson distribution, as expected for shot noise, the mean ( $\mu$ ) and the variance ( $\sigma^2$ ) should be equal. In a visual example of (different) white dots seen at another day and time utilized as controls, choosing dots with a mean comparable to that of the white dots in question, the resultant  $\sigma^2$  was only 10% off from the Poissonian expectation (B). C and D demonstrate that image areas without noise exhibited sub-Poissonian  $\sigma^2$ s, by similar or greater margins.

The closely related resetting of camera parameters hypothesis (8) is disproven by a pixel intensity behavior correlation map for the “closure” (Fig. 9).

It is not realistic to address the military tests hypothesis (9).

The light reflection hypothesis (10) must be carefully studied, even though it cannot explain why this effect was not observed on other nights, nor can it address the dark spot and its slight correlation with the overcast sky.

Most significantly, if the upper-right dark spot is not within the sky, but something on the dome, it does not explain the multiple corroborative videos close in time, which sometimes included camera rotation, both with/without significant spot motion, as well as the possibly corroborative radiation data. While there were potentially corroborative videos from the same camera, no other camera made an observation which could have settled the crucial question of: internal vs. external? The FLIR cameras, some pointed in the same direction, were inactive at the time due to the power needs of film equipment.

While no single hypothesis fits all of the facts, several will still be tested, for a near-future paper: water drops will be placed and allowed to evaporate,

and objects approximating insects, for testing the water droplet (3) and insect (4) hypotheses. Exposure to multiple different radioactive calibration sources in the lab (at UAlbany) will test the cosmic-ray shower hypothesis (5), along with multi-week dark-box tests, to test the cosmic-ray shower (5) and camera noise (7) hypotheses alike. LEDs plus flashlights shined into water drops are some ways in which we can directly probe the light reflection hypothesis (10). Together, such tests will be important for establishing the baseline behavior of our equipment in the face of common phenomena. Most importantly, using pixel intensity mean, intensity width, spatial spread, and other tests, they will remedy the lack of quantitative analyses for some of the hypotheses dismissed qualitatively, right now. Analyses of publicly-available radar data seeking any evidence for/against real objects present in the sky are presented next.

#### *5.1.1. Doppler Weather Radar*

In an effort to answer the crucial question of whether an internal (to the UFODAP) or external phenomenon had been observed, past data from The Next Generation Weather Radar (NEXRAD, part of NOAA) network covering the contiguous U.S. were accessed. (Three sites of WSR-88D installations had the potential to have measurements for our area of interest.) To the best of the authors' knowledge, this is the first attempt to corroborate UAP camera detection by analyzing data from this data source in a scientific paper. The types of data recorded by the NEXRAD radar system include:

1. Reflectivity
2. Radial velocity
3. Spectral width
4. Correlation coefficient

(1-3) are measured from one beam to the next in "moments." (4) is measured between vertical and horizontal channels. Reflectivity was of particular interest, specifically clutter reflectivity, defined later. Reflectivity (1) is amount of transmitted power reflected back to the radar station. This is usually defined with respect to a reference power 1 m from it. Velocity (2) is the average toward/away from the station. Spectral width (3) corresponds to the directions of the velocity vectors, for detections in one "radar pixel," where low implies high consistency in direction, and high greater randomness. Correlation coefficient (4) is a value describing how uniform the shapes of observed features are. (Rain/snow  $\sim 1$ ; birds/insects  $< 0.8$ .) These variables can help us to determine the characteristics of any object that may be detected: information about its size, shape, and state of motion relative to the radar station.

Clutter is defined as radar reflections which are deemed to be from “non-meteorological events” and filtered out (such as traffic or wind farm clutter). The NEXRAD data set saves these in a separate variable called clutter reflectivity (“clutter\_filter\_power\_removed”). Filtration of clutter is a complicated problem: assumptions have to be made. Typically, all detections with no velocity are filtered out, along with manual filtering for known sources of clutter. Different processes are implemented for different radar beam elevation angles. NEXRAD additionally uses a “fuzzy logic” algorithm [43] for more intelligent filtration, permitting more true meteorological events to be logged.

Using the NWS (National Weather Service) NOAA glossary, we summarize the known levels of non-clutter (weather) reflectivity. A Video Integrator and Processor (VIP) contours radar reflectivity (in dBZ) into six levels:

- VIP 1 (18-30 dBZ) - Light precipitation
- VIP 2 (30-38 dBZ) - Light to moderate rain
- VIP 3 (38-44 dBZ) - Moderate to heavy rain
- VIP 4 (44-50 dBZ) - Heavy rain
- VIP 5 (50-57 dBZ) - Very heavy rain; hail possible
- VIP 6 (> 57 dBZ) - Very heavy rain and hail; large hail possible

If the dark spot was an atmospheric event, then based on camera location and angle it most probably occurred between  $281.1^\circ$  and  $286.4^\circ$  (WNW) from the measurement spot on the Californian coast (Fig. 10). Radar returns between 3:30-4:30 were explored starting with the closest station, KSOX. The hour was divided into 10s bins; one interesting time frame was identified, possessing a detection within a pair of rays determined from analyzing the dark spot’s coordinates on the UFODAP videos, at 04:03:50 PDT. There were, in fact, three points within those rays, only slightly later than the times of interest, having values of 27 dBZ, 29 dBZ, and 29 dBZ, large enough to not be likely “sea” clutter (reflections from movements of the waves). See Figure 11.

The other two nearby stations, KNKX and KVTX, were also considered. The former was not sweeping the area at the same time, and the closest sweep in time does not detect anything identified as clutter within the angles of interest. The latter swept through at almost the same time and at a relevantly close elevation, but did not have any detections. This may still be consistent with the KSOX observation, as radar pixels (*range gates*) get larger the further away they are from the detector. Small objects may get washed out when sufficiently far from the station. Range gate is the area encompassed by one radar pixel; it becomes larger with increasing distance from the radar site, as the beam expands, moving away from the source. So resolution decreases with distance from the site. At 30 mi. resolution is  $1 \text{ km}^2$  for a WSR-88D.

One can ask how interesting our KSOX frame is. Echoes from objects like buildings and hills appear in almost all radar reflectivity images. This ground clutter generally appears within a radius of 25 mi. of a site, as a roughly circular region patterned after the surface roughness of the terrain. Radar returns from animals or aircraft are also not uncommon. The apparent intensity and aerial coverage of these features are partly dependent on radio propagation conditions, but they usually appear within 30 mi. of the station and produce reflectivity of  $<30$  dBZ. So, the three points 27, 29, 29 may be considered at least as solid and sizeable of an airborne-clutter reflectivity event as birds, insects, or aircraft. The fact these are relatively high values, and are close in time to the ambiguous videos and 1-2 high-energy particle detections is interesting. Figure 12 addresses the potential explanation of a statistical anomaly.

No corresponding values exist for spectral width or radial velocity (data missing). Correlation coefficients ranged from 0.20-1.05: given their inconsistency, one cannot conclude much from them. Simple, preliminary statistical tests shown in Figure 12 endeavor to answer how common high reflectivity is within background data. We defined three sets of rays: the rays for the dark spot, control rays 1 adjacent but at higher angles and control rays 2 adjacent but at lower angles, always preserving the same angular width. The data were obtained from other dates for the same hour (3:30-4:30am) at time scales of:  $\pm 3$  days,  $\pm 6$  months (winter vs. summer), and  $+1$  year (data from the year before were found to not include a clutter reflectivity variable).

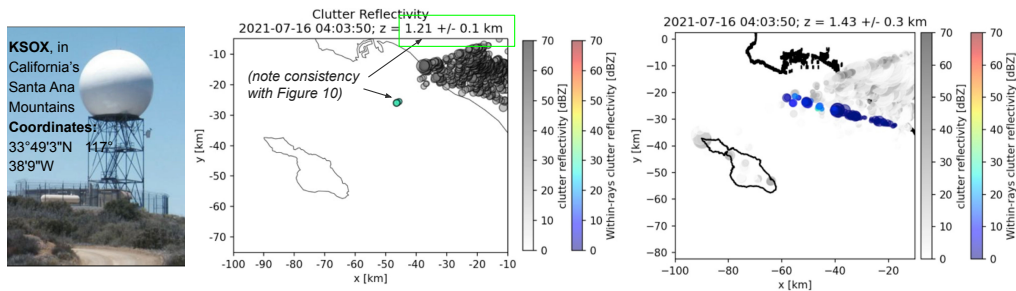


Figure 11: Left: KSOX. Middle: All of its detections within the dark-spot rays in color; all other detections in B&W. Signals below 25 dBZ (default) were filtered out to ensure only strong ones are displayed. Our plot visualizes radar data differently than is traditional (10s bin rather than full sweep, showing circular markers scaling with reflectivity) to accentuate what is relevant for us. Full-sweep maps confirm the data are the same.  $z$  indicates mean elevation for all detections in the bin. Right: No filter; there are many more detections but most too low in intensity to be objects. A case could be made that the (27-29 dBZ) clutter event could be the densest portion of a then slow weather pattern that the radar algorithm designated as clutter. The following 3 days after this were a monsoon event in the region.



The case can be made that it is remarkable that there are radar hits registered by the closest radar station at approximately the same time and place as the camera dark spot with white dots, but timing was indeed only approximate, and it fell outside of UAPx’s timing resolution by a factor of roughly four (Section 5.4). The altitude ‘ $z$ ’ (of 1.2 km) for the hits (Figure 11, center title) is a factor of three too large to match a hole in the cloud ceiling, unless more distant objects were being viewed through a hole in it. Outside of that context, however, the detections themselves remain statistically insignificant, according to Figure 12. Furthermore, we do not have enough evidence to definitively state that they are a part of the same effect(s)/event(s).

That leaves us with this provisional conclusion: that the 27-29 dBZ blips are not inconsistent with the videos and Cosmic Watch, *i.e.*, neither corroborating nor contradicting a non-null hypothesis, or one of the ten involving aerial solids. But now a framework for this sort of analysis is in place, opening doors for comparisons at other locations where there are UAP-concurrent data, to aid in accumulation of corroborating data (*e.g.*, on future trips).

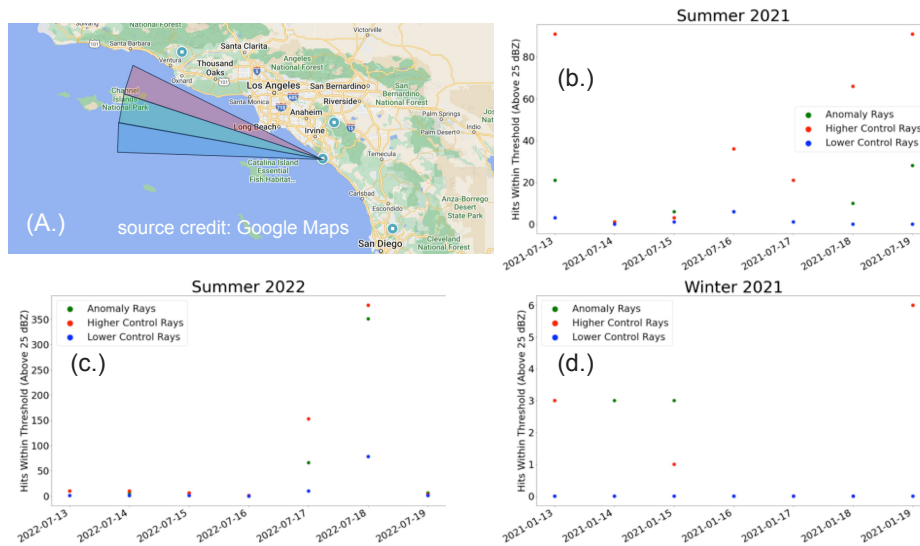


Figure 12: (A.) An approximate visualization for the “ambiguity’s rays” (centered, green), Control 1 (red, higher) and Control 2 (blue, lower). (b.-d.) are clutter reflectivity hits above threshold (25 dBZ) at different times, with (b.) corresponding with the UAPx expedition. Day-to-day variability seems lower for the lower-angle control rays, but with many more hits in summer than winter (note y-axis limits). This may suggest seasonal variation. Hits within the “ambiguity” rays are not particularly rare. Many more hits appear in the higher-angle control rays, although this may be influenced by being closer to the shore. The large increase in hits in 2022 indicates year-to-year differences may be significant too, and Summer 2022 has large day-to-day variability (central-rays hits are not more probable).

### 5.2. Night Vision Binoculars: The International Space Station

Some detections were explicable relatively easily, such as the ISS in night vision goggles ( $1\times$  magnification, no zoom). As not all the websites that track its path properly account for the difference between local time and UT (the one ultimately used for Fig. 2 was correct) the ISS was nearly dismissed as a valid hypothesis due to a 1 hour error (daylight saving time). Another error, common in UAP reports, is estimation of size from a single observation sans independent means of knowing distance (like radar [44]), or a reliable reference. Degeneracy between size and distance can be broken by knowing one of the two with certainty, independently, or by  $\geq 2$  observers a greater distance apart than the position resolution of their measuring/recording devices. The degeneracy can be expressed mathematically for an object of angular size  $\theta$ , stating distance  $d$  as a function of physical size  $s$  (or, vice versa) as:

$$s = d \tan(\theta) \text{ or } d = s \cot(\theta),$$

$$\text{where } \theta = \iota p \text{ and } \iota = \frac{p_{\mu m}}{f_{mm}} \text{ 206.265 arcseconds} \quad (7)$$

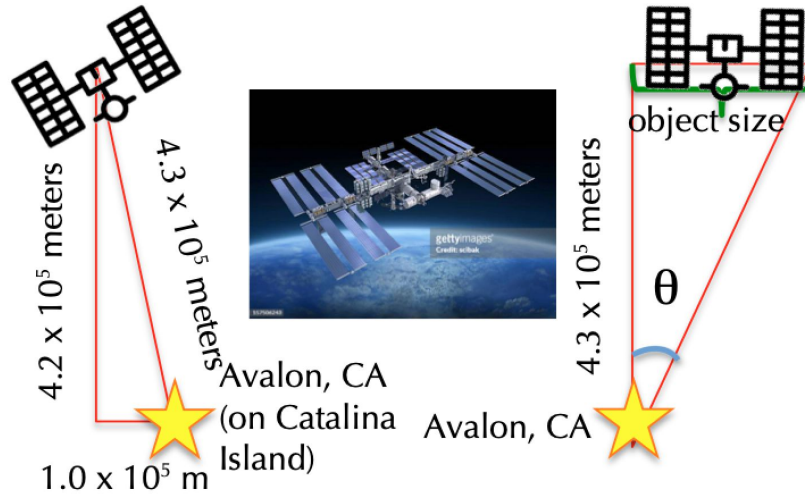


Figure 13: Left: A triangle possessing a base of  $10^5$  m, the distance from Figure 2 between the observer position and the ISS across the Pacific Ocean. The height of this triangle is the ISS' altitude above sea level at the time. Right: A triangle formed from the hypotenuse of the left triangle, and the object in 1D, used to determine its physical size using its angular size in a camera image. As the two spotters were not a sufficient distance apart (at star) for reasonable triangulation, this is merely a consistency check, as there is a degeneracy between length and distance. The length matches the ISS within errors, if its altitude was assumed. This trigonometric exercise serves as a foundation for future UAP work.

Here,  $\iota$  was the number of arcseconds per pixel and  $\theta$  is equal to that multiplied by  $p$ , the object's size in the image, in pixels, across one dimension, with  $p_{\mu m}$  being the physical size of one pixel in microns within the camera's sensor, and  $f_{mm}$  effective camera focal length, in mm. (See Figure 13.) The degeneracy is clear given:  $\theta \approx s/d$ . A distant UAP (at a large  $d$ ) very great in size (large  $s$ ) can be mistaken for something much closer (at small  $d$ ) but also far smaller (small  $s$ ), so that, while it shouldn't be discarded, eyewitness testimony, regarding UAP lengths and distances specifically, must be treated with caution.

Geometric calculations of the length, speed, and shape of the object spotted by night vision, further confirming its identification as the ISS, follow below. (So, they yielded another important lesson learned.) The properties of one of the phones used to record the object (iPhone 11 pro max) were  $1.4 \mu m$  pixel size and 26 mm focal length, leading to 11 arcseconds per pixel. As the object was  $\sim 5$  pixels across (its "core" only) this led to an angular size determination of  $(11 \text{ arcseconds/pixel})(5 \text{ pixels}) = 55 \text{ arcseconds} = 0.015 \text{ degrees} = 2.6 \times 10^{-4} \text{ radians}$ .

$\theta = 2.6 \times 10^{-4} \text{ radians}$  justifies the small angle approximation of  $\tan(\theta) \approx \theta$  so that the object's size can be calculated as

$$s = (4.3 \times 10^5 \text{ m})(2.6 \times 10^{-4} \text{ radians}) \approx 110 \text{ m}. \quad (8)$$

This result should be compared with the actual ISS size of 108 m. The size is only a match to the ISS when using the brighter central feature of the ellipse that was observed (assuming that the fuller size was generated by glow from sunlight), but changing this assumption to 10-15 pixels instead still leads to an object  $O(100 \text{ m})$  in size being found.

Translating an angular to a linear velocity can be highly non-trivial, especially for a non-stationary viewing device, not deployed directly underneath a moving object in the sky. In an attempt to quantify the pixel velocity of the object in question (Figure 13), its motion with respect to a background star and the motion of that background star were both considered. Adding these components in quadrature yielded a  $\sim 30 \text{ pixel/s}$  speed. Given  $110 \text{ m} / 5 = 22 \text{ m/pixel}$ , this would imply a (tangential) speed of 660 m/s, or, ten times too small for the ISS. That being said, taking an average over the entire 2-minute-long incident in place of a frame-by-frame analysis of instantaneous velocity is far closer. This less-crude  $\omega$  estimate is based on the time it took for the object to cross the complete FOV:

$$\omega = (80 \pm 10^\circ) / (120 \pm 10 \text{ seconds}) \quad (9)$$

$$= 0.67 \pm 0.15 \text{ degrees/second} \quad (10)$$

$$= (1.4 \pm 0.2) \times 10^{-2} \text{ radians/second} \quad (11)$$

Differentiating Equation (8) one gets

$$\frac{ds}{dt} = (4.3 \times 10^5 \text{ m}) \frac{d\theta}{dt} = (4.3 \times 10^5 \text{ m})(\omega) \quad (12)$$

$$= 6,000 \pm 1,000 \text{ m/s} = v \quad (13)$$

which compares favorably with the actual ISS velocity at the time, 7660 m/s.

Lastly, consider the approximate shape of the object. Our best visual estimate of aspect ratio was about 1.5 (but definitely not 1:1). The actual aspect ratio of the ISS is about 1.4-2 (it is orientation-dependent).

### 5.3. FLIR *ThermaCams*

The most effort was devoted to the  $8 \times 75 = 600$  hours of FLIR camera recordings. Objects in thermal equilibrium with the environment are difficult to see and craft using conventional propulsion or animals possessing internal heating mechanisms such as avians or mammals would appear hot, but cold objects would be ambiguous.

Two minutes-long incidents occurred in which dozens of objects seemingly “rained” into the ocean, heating it. The UFODAP failed to provide any corroborative detections for these events despite being operational and pointing in the same direction, except for single-pixel triggers suggestive of noise. An exotic answer is signature management, but all of these tracks were observed in only a single camera. They did not seem to be from dead bolometers, which would manifest as permanent white or black pixels (observed in other cameras), nor bolometric discharges, which would appear as localized clusters of white (hot) pixels. Two independent thermal-imaging experts from different manufacturers (at Raytheon and Teledyne) consulted by UAPx, upon review of our two relevant short FLIR video clips, arrived at the same conclusions. Without consulting each other, both in their professional opinions concluded that what we had encountered was a common rastering glitch. Despite their banal interpretation [55], they are not willing to be identified due to the continuing taboo against the study of UAP. This observation, as well as other glitches and example events, can be seen in Figure 14.

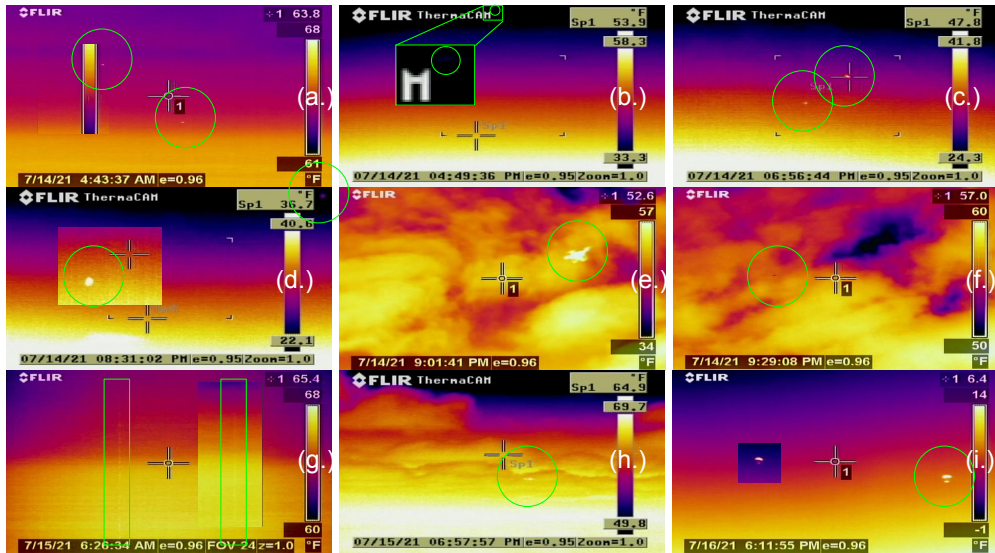


Figure 14: Example FLIR events taken from different cameras, days, and times, in chronological order from left to right and row by row downward, with C-TAP detections circled or boxed. Descriptions begin with the upper left. (a) 7/14 4:43:37am: White (color meaning off-scale hot) patch that is likely a known type of camera glitch, a bolometric discharge, with inset of an example of another one in a different position a few minutes later, also only lasting a few frames. (b) 7/14 4:49:36pm: Faint pixel cluster which traversed the screen in a straight-line path across the top, reading as very cold, with zoom-in inset for easier viewing. This is an example of an event not caught through human viewing, due to being both faint and at the screen's edge. This was most likely an international flight. (c) 7/14 6:56:44pm: A pair of airplanes caught in the same frames, one landing and one taking off from an LA-area airport. (d) 7/14 8:31:02pm: Example image of the Moon, at upper right, and in the inset the Moon seen again, at a different day and time and in a different camera unit. This example illustrates how an identical object (due to an immense distance in this case of course) can appear at different temperatures, depending upon environmental factors, making an absolute determination of temperature from FLIR a challenge. (e) 7/14 9:01:41pm: Standard quad-copter drone, used to film roof scenes in the documentary film *A Tear in the Sky*. (f) 7/14 9:29:08pm: An incident that remains unexplained, a red (false color) oblong shape which endured for approximately 3 frames. While similar in size and shape to a bolometric-discharge camera glitch, it reads cold, not maximally hot. (g) 7/15 6:26:34am: Vertical hot streak, one example of several around the same time frame, originally mistaken for rapidly-moving objects falling into the ocean, but ultimately identified as correlated (temporal) columnar noise. The inset is an example from 9:21am the same morning in the same camera. (h) 7/15 6:57:57pm: Helicopter flying below clouds. (i) 7/16 6:11:55pm: Para-sailor  $O(100\text{ m})$  in front of the cameras, observed in multiple units. The inset shows the same recreating individual at the same time from a different point of view. Other interesting events not pictured include transient points of light most likely beacons on oil rigs in the channel bleeding into the IR, and a wingless ellipse which U-turned.

As mentioned already within Section 3.4, moving forward we will plan to use fewer, but far more portable, thermal cameras – specifically, the Teledyne FLIR One Pro, which will be cooled down manually, and be simultaneously charging and operating to allow for multiple-hour recordings. The calibration campaign before any next expedition will involve phase transitions: of water and other substances at different distances and atmospheric conditions. The FOV will be much more limited, but a gimbal moving to follow targets identified and tracked by the UFODAP (running different software such as Sky-Hub’s) will compensate for this deficiency. Figure 15 has example imagery.

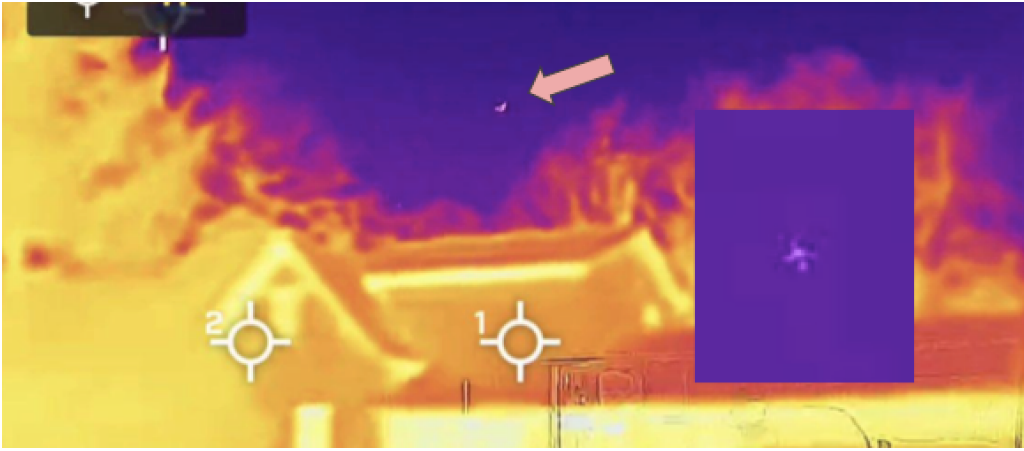


Figure 15: Example of the Moon (crescent phase) in the new UAPx (mini)FLIR for smart-phone. This should be compared to its appearance in Fig. 14d (left column, center row). The resolution has improved from 360p to 1080p, and the device also comes with a CCD overlay from a built-in second (visible-light) camera. Inset: Demonstration of how even distant airplanes (overhead) are more obvious in shape now, no longer generic white (hot) ellipsoids without any well-defined wings distinct from the fuselage (leading to UAP claims).

#### 5.4. Radiation: Counts and Energies

Multiple statistical outliers were identified within the 205,920 s of Cosmic Watch livetime (89,220 individual detections), as two types: high-rate excursions (time-binning dependent) and higher energies (in Figure 16). In the former case, most appeared to be correlated with increased solar activity from the week of the expedition based upon data from the scientific instrument of ERNE (Energetic and Relativistic Nuclei and Electrons) for measuring energetic particles, deployed on the SOHO (Solar and Heliospheric Observatory) spacecraft, as well as data from particle detectors on GOES (Geostationary Operational Environmental Satellite), or NASA geomagnetic storm alerts.

Name	times [ms]	Voltage [mV]	*E [MeV]	time stamp [Pacific]	#	times [ms]	rate [Hz]	time stamp [Pacific]
alpha	180417934	890.81	43.37	2021-07-16 04:01:30.731	1	34686181	2.9842	2021-07-14 11:34:09.333
beta	104386879	882.02	42.95	2021-07-15 06:55:06.211	2	202361285	2.5368	2021-07-16 10:07:00.459
gamma	64171593	827.54	40.29	2021-07-14 19:45:16.984	3	194442566	2.6983	2021-07-16 07:55:06.425
delta	153565984	827.54	40.29	2021-07-15 20:34:15.976	4	15855123	2.3381	2021-07-16 18:09:41.611
epsilon	139133218	774.66	37.72	2021-07-15 16:33:51.686	5	202360018	2.2841	2021-07-16 10:06:59.170
zeta	126464210	742.25	36.14	2021-07-15 13:02:49.962	6	30625914	2.4091	2021-07-14 10:26:31.590
eta	26718095	691.56	33.67	2021-07-14 09:21:26.161	7	22451931	2.151	2021-07-16 19:59:34.168
theta	58282958	663.75	32.32	2021-07-14 18:07:12.009	8	30625839	2.0773	2021-07-14 10:26:31.536
iota	151841558	622.01	30.29	2021-07-15 20:05:32.647	9	15854498	2.2467	2021-07-16 18:09:40.988
kappa	63362606	622.01	30.29	2021-07-14 19:31:48.518	10	172035664	2.1515	2021-07-16 01:41:53.835
lambda	114215744	618.81	30.13	2021-07-15 09:38:49.057	11	22452317	1.9654	2021-07-16 19:59:34.551
mu	91375860	611.5	29.77	2021-07-15 03:18:23.521	12	166331896	2.2193	2021-07-16 00:06:53.750
nu	30776611	611.5	29.77	2021-07-16 22:18:13.300	13	19077443	2.0517	2021-07-14 07:14:10.257
xi	88924223	611.5	29.77	2021-07-15 02:37:33.476	14	22452738	1.9681	2021-07-16 19:59:34.975
omicron	167701797	611.5	29.77	2021-07-16 00:29:42.772	15	58642339	1.9596	2021-07-14 18:13:11.161
pi	112362949	559.34	27.23	2021-07-15 09:07:57.410	16	176285415	1.7924	2021-07-16 02:52:40.886
rho	34100707	526.8	25.65	2021-07-14 11:24:24.253	17	30626142	1.9327	2021-07-14 10:26:31.818
sigma	181418488	526.8	25.65	2021-07-16 04:18:10.645	18	49781612	1.7813	2021-07-14 15:45:35.457
tau	209664285	522.36	25.43	2021-07-16 12:08:39.012	19	176284730	1.8512	2021-07-16 02:52:40.199
upsilon	112682231	515.83	25.12	2021-07-15 09:13:16.491	20	97141358	1.8396	2021-07-15 04:54:25.313
phi	208838805	509.46	24.81	2021-07-16 11:54:54.037	21	4595842	1.8325	2021-07-16 15:02:08.764
chi	154319951	486.08	23.67	2021-07-15 20:46:49.464	22	93544511	1.9069	2021-07-15 03:54:30.756
psi	18978537	484.8	23.60	2021-07-16 19:01:43.055	23	8834094	1.7902	2021-07-16 16:12:44.589
omega	77764551	479.13	23.33	2021-07-14 23:31:41.059	24	17784811	1.734	2021-07-14 06:52:38.476
alef	52764136	479.13	23.33	2021-07-14 16:35:16.347	25	166427750	2.0101	2021-07-16 00:08:29.522
bet	25897385	469.96	22.88	2021-07-14 09:07:45.951	26	147761593	1.8409	2021-07-15 18:57:35.248
gimel	125349718	468.76	22.82	2021-07-15 12:44:16.143	27	36111066	2.2411	2021-07-14 11:57:53.337
dalet	180166166	468.76	22.82	2021-07-16 03:57:19.126	28	36112435	1.9728	2021-07-14 11:57:54.681
he	49856157	454.77	22.14	2021-07-14 15:46:49.968	29	18659089	1.9508	2021-07-14 07:07:12.167
waw	84533357	450.26	21.92	2021-07-15 01:24:25.451	30	113418740	1.9501	2021-07-15 09:25:32.553
zayin	133624049	445.84	21.71	2021-07-15 15:02:05.439	31	94968585	1.9124	2021-07-15 04:18:13.927
chet	195330393	442.02	21.52	2021-07-16 08:09:53.778	32	168575790	1.8968	2021-07-16 00:44:16.202
tet	36111066	432.99	21.08	2021-07-14 11:57:53.337	33	137780125	1.8797	2021-07-15 16:11:19.270
yod	9996749	428.33	20.85	2021-07-14 04:42:55.514	34	43786521	1.8639	2021-07-14 14:05:44.045
kaf	119997857	423.75	20.63	2021-07-15 11:15:07.562	35	98785922	1.8515	2021-07-15 05:21:48.830
lamed	83980421	421.74	20.53	2021-07-15 01:15:12.885	36	200700784	1.8491	2021-07-16 09:39:20.938
mem	30924941	415.31	20.22	2021-07-14 10:31:30.454	37	114440914	1.8409	2021-07-15 09:42:34.088
nun	2175958	414.82	20.20	2021-07-16 14:21:50.430	38	92289252	1.8365	2021-07-15 03:33:36.299
samech	183430366	414.82	20.20	2021-07-16 04:51:41.217	39	1923348	1.8365	2021-07-14 02:28:27.444
ayin	200428591	414.82	20.20	2021-07-16 09:34:48.913	40	175304197	1.7886	2021-07-16 02:36:20.303
pe	37968798	407.61	19.84	2021-07-14 12:28:49.945	41	153722459	1.7565	2021-07-15 20:36:52.361
tsadik	203682719	407.61	19.84	2021-07-16 10:29:01.080	42	92289386	1.7565	2021-07-15 03:33:36.457
qof	176631923	406.66	19.80	2021-07-16 02:58:27.181	43	11208719	1.7559	2021-07-16 16:52:17.916
resh	196647487	400.12	19.48	2021-07-16 08:31:50.105	44	172037136	1.7197	2021-07-16 01:41:53.329
shin	128378255	399.2	19.44	2021-07-15 13:34:42.837	45	174118627	1.7176	2021-07-16 02:16:35.501
tav	44438645	397.37	19.35	2021-07-14 14:16:35.766	46	58642926	1.7047	2021-07-14 18:13:11.748

Figure 16: Left: List of high-energy events labeled in Greek then Hebrew letters high-low (top-bottom), converted from raw pulse area, and timestamps in ms converted into local time for the final column. Bold lines are more ambiguous, as they cannot be attributed to a CME (Coronal Mass Ejection) or a solar flare. 2 MeV is the expected average (muons), while 8 MeV is the maximum for most natural Earthly sources of radiation. Yellow coloring indicates suspected temporal correlations of multiple detections high in energy, and orange indicates potential clusters of events high in both energy deposited and count rate. Right: A similar table but for the highest rates, numbered from highest to lowest, for the week. (These will be further probed in a later paper about Cosmic Watches for both UAP as well non-UAP research, such as solar physics.) The average was  $\sim 0.5$  Hz (in non-coincidence mode) for the older version of the unit used by UAPx. The bold and non-bold fonts, and color scheme of yellow and orange highlights, have the same meaning as in the left table.

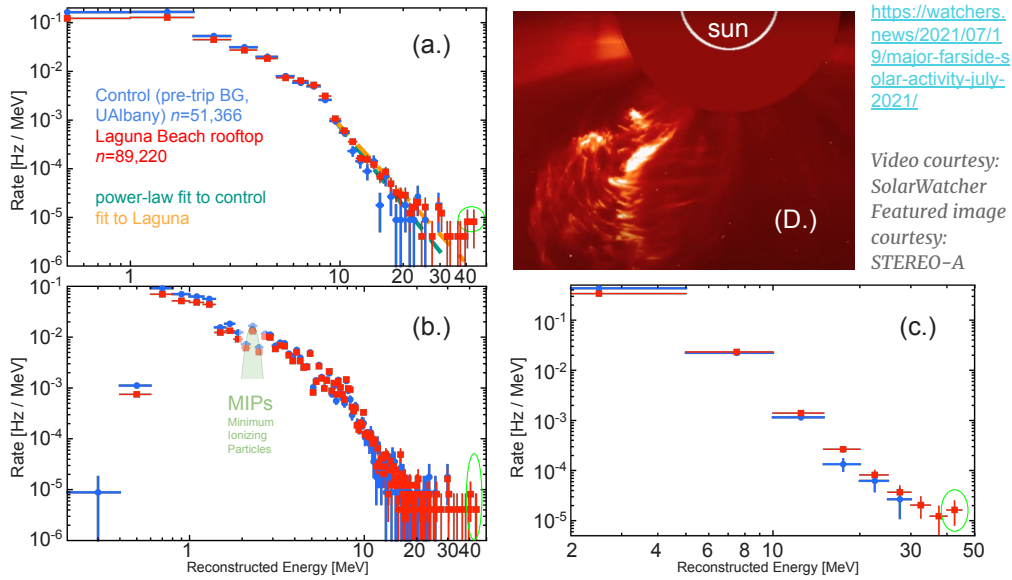


Figure 17: (a.) Pre-expedition control data as cyan diamonds and Laguna Beach, California data as red squares from the MIT Cosmic Watch, with a coarse binning. Power laws, as expected, are fit to them above the cut-off for terrestrial radiation. (b.) The same data sets but with finer binning, enabling one to see the roll-off at low energies due to the device’s efficiency, and the feature (in green) near 2 MeV which corresponds to  $\sim 2$  MeV/cm minimum ionizing particles (MIPs) from the natural background of cosmic rays, primarily muons, which were used to determine the energy scaling from raw SiPM scintillation pulse area or ADC counts. (This peak is easier to see in earlier data [5, 4, 6]). (c.) The same data again but with an in-between binning. Post-trip control data exist but with a replacement unit, due to the original one breaking down, so they are not shown due to being an unreliable comparison (newer versions have a different *i.e.* higher efficiency). In plots (a.-c.), a light green oval encircles the four events above 40 MeV  $\alpha$ ,  $\beta$ ,  $\gamma$ , and  $\delta$ . (D.) Photograph of solar activity at the time of the UAPx trip. It cannot explain those four events, but may explain some higher-rate events, even though this activity was on the far side of the Sun, pointed away from Earth, as a result of indirect “backwash” (not a strong explanation).

These will be part of a future article, on the first such use case (solar) of a Cosmic Watch. For the higher energies ( $E_s$ ), at least four (single-interaction) particularly ambiguous events were identified, visible in Figure 17 even with different binning, especially in comparison with the control data of only 40% less livetime: two at 43 MeV (labeled as  $\alpha$  and  $\beta$  in Figure 16) and two at 40 MeV ( $\gamma$  and  $\delta$ ). As a result of the intrinsic features of MIT’s Cosmic Watch, the particle type is not known, so these are only electron-equivalent  $E_s$ , due *e.g.* to quenching factors for nuclear recoils like those from cosmic-ray neutrons. They may also be in MeV/cm, not MeV, if triggers were part of long-



track vertical particles passing through 1 cm of plastic scintillator. In spite of the potential excess near 40 MeV in Figure 17 compared to control data, by themselves these events are not statistically significant ( $2\text{-}3\sigma$  max *cf.* control data or either fit), and are explicable as cosmic rays from astrophysical phenomena. They routinely exceed 40 MeV by many orders of magnitude. But, one coincidence caught our attention, as we discuss next – the  $\alpha$  event seemed to be close in time to at least one UFODAP video (3:59:24 am, Section 5.1).

We can estimate the “accidental coincidence” rate or  $R_{AC}$  for videos with high-energy detections at/near  $\sim 43$  MeV, by applying the standard formula for this from particle physics, for a pair of measuring devices:

$$R_{AC} = 2 r_{UD} r_{CW} \Delta t. \quad (14)$$

The detection rates  $r_{UD}$  and  $r_{CW}$  for the UFODAP and Cosmic Watch were:

$$r_{UD} = (1,716 \text{ files}) / (396,300 \text{ s}) = 0.004330 \text{ Hz} \quad (15)$$

$$r_{CW} = 1.65 \times 10^{-6} \text{ Hz} \quad (16)$$

Eqn. (15) is rate, but looking at the inverse the mean is 176s between videos (so, 117s is sensible; 11s is an outlier, p. 15). Eqn. (16) comes from the appropriate bin in Figure 17, accounting for  $E$  resolution. While the video closest in time to event  $\alpha$  was 0.267s long, we conservatively set  $\Delta t = 60$ s, our best retroactive estimate of the maximum time difference amongst devices. This leads us to a key lesson learned, already mentioned in Section 4.2, of the need for a second-level time synchronization in all equipment, to permit precision calculations of coincidence timing. (Subtracting the 3:59 am from Section 5.1 from the first line in Figure 16 (4:01) yields 127s, a similar value.) The result from Eqn. (14) is then only  $0.9 \mu\text{Hz}$ . Superficially, this seems to be a remarkably low rate; however, the total livetime for which both the UFODAP and UAPx’s Cosmic Watch were operational concurrently was 194,895 s, leading to an expectation value of 0.2 accidentally-coincident events for the week.

A naïve calculation would say that  $0.2/1716$  is a  $10^{-4}$  fractional chance or 0.01% odds ( $> 3.5\sigma$  one-tailed or two-tailed normal probability distribution), but this would neglect the large number of Cosmic Watch events as well as the total livetime. A statement like this would have required better synchronization to reduce  $\Delta t$ , with the SiPM pulse widths and video times already short, or a less sensitive UFODAP trigger. The more correct calculation follows: the

expectation value (average) for the number of accidentally-coincident events, for data collection lasting time  $\tau$ , is  $\langle AC \rangle = R_{AC}\tau$ , with Poisson probability

$$P = \frac{\langle AC \rangle^k}{k!} e^{-\langle AC \rangle} \approx \langle AC \rangle \text{ for } \langle AC \rangle \ll 1 \text{ and } k = 1 \quad (17)$$

of happening  $k$  times during the trip. By taking into account the duration of an excursion (or, the total number of detections) this eliminates the mistake in assuming, for example, that a “1 in a million” detection is anomalous when one has 1 million or more data points (the “Look Elsewhere Effect.”) In the full treatment, Eq. (17), we see the  $P$  of our coincidence was  $\approx 20$  not 0.01%.

For simplicity, if all triggering rates are sufficiently small, so they are well modeled by Poisson functions, and each sensor in usage can be approximated as having a temporal width (relevant time scale) much shorter than the time synchronization uncertainty, we recommend utilizing Equations (14) and (17) in all multi-modal studies of UAP. If three or more sensors are employed by a team on an expedition we recommend generalizing Equation (14) to  $N$  units with unique backgrounds  $r_i$  (and/or public data sets) and resolution  $\Delta t$  [15]

$$R_{AC} = N \prod_{i=1}^N r_i \Delta t^{N-1} \quad (18)$$

As a result of Equation (17), our initial ambiguity is ultimately not classifiable as an anomaly statistically speaking, when using the two-device version of Equation (18), and there exist systematics which may decrease any improbability even further, such as the existence of events  $\beta$ ,  $\gamma$ , and  $\delta$  of comparable energies as  $\alpha$  lacking in similar UFODAP observations, the smaller exposure time for background data, and a lack of a non-speculative/exotic mechanism which would link a correlation with causation. That said, there are also other considerations which may increase it if different analysis choices are made:

- Counting all videos in the coincidence calculation, instead of just those within the Cosmic Watch livetime, and only those with inexplicable (at least initially) video frames, *qualitatively* ambiguous in a single sensor
- The overall cosmic-ray rate should have decreased at the lower latitude: Laguna Beach *cf.* Albany. (This oddness is the clearest in Fig. 17c.)
- There is another high-energy event, from 3:57:19 am, labeled as dalet in the table in Figure 16 (22.8 MeV, expected to occur at  $2 \times 10^{-5}$  Hz rate)

that may not only be correlated with another UFODAP recording, but be related to the same incident under discussion. Multiplying 0.2, the highest probability we found for  $\alpha$  overlapping with the UFODAP, with the probability of 0.1 for the 22.8 MeV event to occur within 3 seconds of a different video =  $(2 \times (4.33 \times 10^{-3}) \times (2 \times 10^{-5}) \times 3 \times (2 \times 10^5))$ , along with a probability of 0.02 for those two radiation measurements occurring within 4 minutes of each other  $(2 \times (2 \times 10^{-5}) \times (1 \times 10^5) \times 240 \times (2 \times 10^5))$ , yields  $4 \times 10^{-4}$  ( $> 3\sigma$  again). But, this may be an unjustified multiplication of a long string of probabilities, if causation linkage can't be established, even if speculative, for treatment as a single incident.

- Other potential corroborations, such as unusual radiation readings at global monitoring stations, may be relevant if near-simultaneous.

A simulation took into account the UFODAP trigger rate, Cosmic Watch rate in relevant energy bins, lengths of UFODAP recordings, pulse widths in the Cosmic Watch, synchronization uncertainties, uncertainties in all mean quantities, and all effects above. The result was  $> 3\sigma$  significance once again, for an accidental coincidence of three videos with two high-energy events.

## 6. Conclusions

In light of the possibilities, our most intriguing event appears almost by definition to be “ambiguous”; changing interpretations change the statistical significance. That has inspired us to recommend a general plan for this field. We suggest that (scientific) UAP researchers adopt the following conventions: An **ambiguity** requiring further study is a coincidence between two or more detectors or data sets at the level of  $3\sigma$  or more, with a declaration of genuine **anomaly** requiring (a HEP-inspired)  $5\sigma$ , combining Equations (18) and (17). (HEP = High-Energy Physics.) Coincidence here is defined as “simultaneity” within the temporal resolution, and spatial when germane. This way, one rigorously quantifies the meaning of extraordinary evidence, in the same way it has been done historically by particle physicists, who have established a very high bar to clear. The statistical significance must be defined relative to a null hypothesis, in our case accidental coincidence, combined with causally-linked hypotheses, like cosmic rays striking camera pixels. For cases where statistical significance is difficult to determine, we recommend one defines ambiguity based upon the number of background events expected, where 1 event is the border. For example, if  $< 1$  event is expected to be nearly simultaneous for a particular pair of sensors, but  $\geq 1$  events are detected, then they should each be inspected, as time permits, especially qualitatively ambiguous incidents.

UAPx mounted an expedition in July of 2021 to a (suspected) UAP hot-spot with UAlbany SUNY physicists. Exotic ideas like UAP radiation were entertained, balanced by a strenuous pursuit of skepticism. With one possible exception, ambiguous observations ended up being identifiable. At this point, none can be classified as true anomalies, although further study of remaining ambiguities may alter this conclusion. The greatest successes from this work were equipment stress-testing in the field, creation of new software of broad applicability, and valuable lessons for any future field work. We recommend at least two of each type of sensor, and at least two distinct sensor types. Most significantly, recommendations have been made for a novel research area, for establishing quantitative rigor in the definitions of ambiguities vs. anomalies. Our results thus far may be best labelled as “null,” but the history of science teaches us the value of such results [17], and of robust eliminative deduction. New excursions, to Catalina for reproducibility, and elsewhere, will include improvements to both equipment/methods, recognizing others’ past work.

## 7. Acknowledgements

The authors acknowledge OMnium Media for providing the funding for all the Laguna/Catalina field work. In addition, we’d like to thank Seattle area technician David Mason for use of his FLIR cameras, night vision, and other equipment. We also thank David Altman and Michael Hall for serving as the island team. We thank iHeartMedia for financial support, and iHeart’s podcaster/reporter Claude Brodesser-Akner. For manuscript reviews, we are indebted to two anonymous academics, and for FLIR review to two professionals. We also thank retired electrical engineers Candy and Ralph Segar for efforts in analysis and review. We thank Caroline Cory, Lenny Vitulli, Michael Soto, and the entire film crew for “A Tear in the Sky.” We also thank William Shatner for his refreshing skepticism. We thank a Warning Coordination Meteorologist in the NOAA/NWS’s San Diego office, Alexander Tardy, several other (anonymous) meteorologists, and one (anonymous) Knuth group alum, for their radar analysis assistance. We thank Alex Garcia for media relations. We thank everyone involved with the History channel show *The Proof is Out There* for covering UAPx, especially Miguel Sancho and Genevieve Wong.

## References

- [1] I. F. Albuquerque and A. Chou. A faraway quasar in the direction of the highest energy Auger event. *Journal of Cosmology and Astroparticle*

- Physics*, 2010(08):016–016, Aug. 2010. URL <http://dx.doi.org/10.1088/1475-7516/2010/08/016>.
- [2] E. O. ANGÜNER. Exploring the high-energy frontiers of the Milky Way with ground-based gamma-ray astronomy: PeVatrons and the quest for the origin of Galactic cosmic-rays. *Turkish Journal of Physics*, 47(2): 40–92, Jan 2023. doi: 10.55730/1300-0101.2738. URL <https://doi.org/10.55730%2F1300-0101.2738>.
- [3] F. Aubin, M. Auger, M.-H. Genest, G. Giroux, R. Gornea, R. Faust, C. Leroy, L. Lessard, J.-P. Martin, T. Morlat, M.-C. Piro, N. Starinski, V. Zacek, B. Beltran, C. B. Krauss, E. Behnke, I. Levine, T. Shepherd, P. Nadeau, U. Wichoski, S. Pospisil, I. Stekl, J. Sodomka, K. Clark, X. Dai, A. Davour, C. Levy, A. J. Noble, and C. Storey. Discrimination of nuclear recoils from alpha particles with superheated liquids. *New Journal of Physics*, 10(10):103017, Oct. 2008. ISSN 1367-2630. doi: 10.1088/1367-2630/10/10/103017. URL <http://dx.doi.org/10.1088/1367-2630/10/10/103017>.
- [4] S. Axani, K. Frankiewicz, and J. Conrad. The CosmicWatch desktop muon detector: a self-contained, pocket-sized particle detector. *Journal of Instrumentation*, 13(03):P03019–P03019, Mar 2018. doi: 10.1088/1748-0221/13/03/p03019. URL <https://doi.org/10.1088%2F1748-0221%2F13%2F03%2Fp03019>.
- [5] S. N. Axani. The Physics Behind the CosmicWatch Desktop Muon Detectors, 1908.00146.
- [6] S. N. Axani, J. M. Conrad, and C. Kirby. The desktop muon detector: A simple, physics-motivated machine- and electronics-shop project for university students. *American Journal of Physics*, 85(12):948–958, Dec 2017. doi: 10.1119/1.5003806. URL <https://doi.org/10.1119%2F1.5003806>.
- [7] L. E. Catoe, K. Rodgers, and L. A. Shepard. *UFOs and Related Subjects: An Annotated Bibliography*, volume 19.2. US Government Printing Office, 1969.
- [8] J. Cen, P. Yuan, and S. Xue. Observation of the optical and spectral characteristics of ball lightning. *Physical Review Letters*, 112(3):035001, 2014.

- [9] A. E. Chavarria et al. Measurement of the ionization produced by sub-keV silicon nuclear recoils in a CCD dark matter detector. *Physical Review D*, 94(8), Oct 2016. doi: 10.1103/physrevd.94.082007. URL <https://doi.org/10.1103/physrevd.94.082007>.
- [10] G. M. Clemence. Review of the University of Colorado Report on Unidentified Flying Objects by a Panel of the National Academy of Sciences. Technical report, National Academy of Sciences, Washington DC, 1969.
- [11] H. Cooper, R. Blumenthal, and L. Kean. Glowing Auras and ‘Black Money’: The Pentagon’s Mysterious U.F.O. Program. *The New York Times*, A:1, 2017.
- [12] B. Coudurier, C. E. Hoyos, M. Niedermayer, P. B. Mahol, T. Borgmann, T. Härdin, S. Liu, G. Doshi, and A. Khirnov. FFmpeg, October 2013. URL <https://www.ffmpeg.org/>. Accessed Nov 1, 2023.
- [13] D. Coumbe. *Anomaly. A scientific exploration of the UFO phenomenon*. Rowman & Littlefield Publishers, Lanham MD, 2022.
- [14] L. Davidson. *Flying Saucers: An Analysis of the Air Force Project Blue Book Special Report No. 14*. Ramsey-Wallace Corporation, 1966.
- [15] C. Eckart and F. R. Shonka. Accidental Coincidences in Counter Circuits. *Phys. Rev.*, 53:752–756, May 1938. doi: 10.1103/PhysRev.53.752. URL <https://link.aps.org/doi/10.1103/PhysRev.53.752>.
- [16] G. Fallas. Vehicle interference project. In C. F. Lockwood and A. Pace, editors, *BUFORA*. British UFO Research Association, 1979.
- [17] A. Franklin and R. Laymon. The Michelson–Morley experiments of 1881 and 1887. In *Measuring Nothing, Repeatedly*, 2053-2571, pages 7–1 to 7–24. Morgan & Claypool Publishers, 2019. ISBN 978-1-64327-738-7. doi: 10.1088/2053-2571/ab3918ch7. URL <https://dx.doi.org/10.1088/2053-2571/ab3918ch7>.
- [18] C. C. French, U. Haque, R. Bunton-Stasyshyn, and R. Davis. The “Haunt” project: An attempt to build a “haunted” room by manipulating complex electromagnetic fields and infrasound. *Cortex*, 45(5): 619–629, 2009.

- [19] F. Freund. Co-seismic earthquake lights: the underlying mechanism. *Pure and Applied Geophysics*, 176(8):3439–3450, 2019.
- [20] F. T. Freund. Rocks that crackle and sparkle and glow: strange pre-earthquake phenomena. *Journal of Scientific Exploration*, 17(1):37–71, 2003.
- [21] P. R. Hill. *Unconventional Flying Objects: A Former NASA Scientist Explains How UFOs Really Work*. Hampton Roads Publishing, 2014.
- [22] P. R. Hill, R. M. Wood, and D. Donderi. *Unconventional Flying Objects: a scientific analysis*. Hampton Roads, 1995.
- [23] R. Hoffman. Scientific Coalition for UAP Studies, January 2017. URL <https://www.explorescu.org/>. Accessed Oct 31, 2023.
- [24] R. Hopf. What’s in Our Skies?, April 2021. URL <https://www.sky360.org/>. Accessed Nov 1, 2023.
- [25] J. D. McGowan. <https://jeremydmcgowan.com/>, June 2021. URL <https://www.teksynap.com/contracts/ites-3s/>. Accessed Dec. 1, 2023.
- [26] H. Kayal. Scientific and Technological Exploration of Unidentified Aerial Phenomena (UAP). In J. Andresen and O. Torres, editors, *Extraterrestrial Intelligence: Academic and Societal Implications*, pages 87–111. Cambridge Scholars Publishing, 2022.
- [27] H. Kayal, T. Greiner, T. Kaiser, and S. Oehme. Research on Unidentified Aerial Phenomena at the Julius-Maximilians-University of Würzburg. In *AIAA AVIATION 2023 Forum*, page 4100, 2023.
- [28] K. H. Knuth, R. M. Powell, and P. A. Reali. Estimating flight characteristics of anomalous Unidentified Aerial Vehicles. *Entropy*, 21(10):939, 2019.
- [29] D. Letty and the COMETA Asssocation. UFOs and defense: What should we prepare for, 1999.
- [30] A. Loeb and S. Kirkpatrick. PHYSICAL CONSTRAINTS ON UNIDENTIFIED AERIAL PHENOMENA, March 2023. URL <https://1web.cfa.harvard.edu/~loeb/LK1.pdf>. Accessed Oct 31, 2023.

- [31] Loeb, Abraham, on behalf of the Galileo Project, Harvard University. Overview of the Galileo Project, arXiv:2209.02479.
- [32] W. Markowitz. The Physics and Metaphysics of Unidentified Flying Objects: Reported UFOs cannot be under extraterrestrial control if the laws of physics are valid. *Science*, 157(3794):1274–1279, 1967.
- [33] J. M. McCampbell. Physical effects of UFOs Upon People. In *UFOs: 1947-1987, the 40-Year Search for an Explanation*. Fortean Times London, 1987.
- [34] A. Mead, S. Little, P. Sail, M. Tu, W. A. Watters, A. White, and R. Cloete. Multi-Band Acoustic Monitoring of Aerial Signatures. *Journal of Astronomical Instrumentation*, 12(01), March 2023. doi: 10.1142/s2251171723400056. URL <https://doi.org/10.1142/2Fs2251171723400056>.
- [35] A. Meessen. Evidence of Very Strong Low Frequency Magnetic Fields. In *PIERS Proceedings, Moscow, Russia*, 2012. URL <https://api.semanticscholar.org/CorpusID:54980094>.
- [36] MUFON. The MUFON UFO Journal. In *Mutual UFO Network UFO Journal*, 1967. URL <https://mufon.com/>.
- [37] H. Oberth. Lecture notes for Lecture about Flying Saucers, 1954. URL <http://knuthlab.org/library/Oberth-1954.pdf>.
- [38] Office of the Director of National Intelligence. 2022 Annual Report on Unidentified Aerial Phenomena, November 2022. URL <https://www.dni.gov/files/ODNI/documents/assessments/Unclassified-2022-Annual-Report-UAP.pdf>. Accessed Dec. 4, 2023.
- [39] R. Olch. UFODAP, July 2021. URL <http://ufodap.com/>. Accessed Oct 18, 2023.
- [40] C. Poher. Analysis of Radar and Air-Visual UFO Observations on 24 October 1968 at Minot AFB, North Dakota, USA. [explorescu.org/post/analysis-of-radar-and-air-visual-ufo-observations-on-24-october-1968-at-minot-afb-north-dakota-usa](https://explorescu.org/post/analysis-of-radar-and-air-visual-ufo-observations-on-24-october-1968-at-minot-afb-north-dakota-usa), 2005. Accessed: 2019-09-08.



- [41] Popular Military. Air Force Veteran Awarded Full Disability for UFO Exposure, March 2015. URL <https://popularmilitary.com/air-force-veteran-awarded-full-disability-for-ufo-exposure>. Accessed Oct 21, 2023.
- [42] R. Powell, P. Reali, T. Thompson, M. Beall, D. Kimzey, L. Cates, and R. Hoffman. Forensic analysis of Navy Carrier Strike Group Eleven’s encounter with an anomalous aerial vehicle, 2019. URL <https://www.explorescu.org/post/2004-uss-nimitz-strike-navy-group-incident-report>. Accessed: 2019-07-09.
- [43] B. Radhakrishna, F. Fabry, and A. Kilambi. Fuzzy Logic Algorithms to Identify Birds, Precipitation, and Ground Clutter in S-Band Radar Data Using Polarimetric and Nonpolarimetric Variables. *Journal of Atmospheric and Oceanic Technology*, 36(12):2401 – 2414, 2019. doi: <https://doi.org/10.1175/JTECH-D-19-0088.1>. URL <https://journals.ametsoc.org/view/journals/atot/36/12/jtech-d-19-0088.1.xml>.
- [44] M. Randall, A. Delacroix, C. Ezell, E. Kelderman, S. Little, A. Loeb, E. Masson, W. A. Watters, R. Cloete, and A. White. SkyWatch: A passive multistatic radar network for the measurement of object position and velocity. *Journal of Astronomical Instrumentation*, 12(01), Mar 2023. doi: 10.1142/s2251171723400044. URL <https://doi.org/10.1142/s2251171723400044>.
- [45] M. Rodeghier, M. Hynek, and S. H. Longden. *UFO Reports Involving Vehicle Interference: A Catalogue and Data Analysis*. Center for UFO Studies, 1981.
- [46] J. F. Schuessler and R. Pratt. *The Cash-Landrum UFO Incident*. CreateSpace Independent Publishing Platform, 1998. ISBN 978-1519696557.
- [47] S. Singer. *The nature of ball lightning*. Springer Science & Business Media, 2012.
- [48] E. Solano, G. W. Marcy, B. Villarroel, S. Geier, A. Streblyanska, G. Lombardi, R. E. Bär, and V. N. Andruk. A bright triple transient that vanished within 50 minutes, 2310.09035.

- [49] F. St.-Laurent, J. S. Derr, and F. T. Freund. Earthquake lights and the stress-activation of positive hole charge carriers in rocks. *Physics and Chemistry of the Earth, Parts A/B/C*, 31(4-9):305–312, 2006.
- [50] M. Stenhoff. The Existence of Ball Lightning. *Ball Lightning: An Unsolved Problem in Atmospheric Physics*, pages 163–178, 1999.
- [51] M. Szenher, A. Delacroix, E. Keto, S. Little, M. Randall, W. A. Watters, E. Masson, and R. Cloete. A Hardware and Software Platform for Aerial Object Localization. *Journal of Astronomical Instrumentation*, 12(01), Mar 2023. doi: 10.1142/s2251171723400020. URL <https://doi.org/10.1142/s2251171723400020>.
- [52] M. Szydagis. *Dark matter limits from a 15 kg windowless bubble chamber*. PhD thesis, The University of Chicago, 2011.
- [53] T. Taylor. Preliminary Assessment: Unidentified Aerial Phenomena, June 25 2021. URL <https://www.dni.gov/files/ODNI/documents/assessments/Preliminary-Assessment-UAP-20210625.pdf>. Accessed Nov. 09, 2023.
- [54] J. J. Tedesco, G. T. Tedesco, and D. L. Nardo. Eye On the Sky: A UAP Research and Field Study on New York’s Long Island Coast. In *SCU*, 2023. URL doi10.5281/zenodo.8341543.
- [55] Teledyne FLIR. What is a Non-Uniformity Correction (NUC)?, March 2020. URL <https://www.flir.com/discover/professional-tools/what-is-a-non-uniformity-correction-nuc/>. Accessed Dec. 04, 2023.
- [56] M. Teodorani. A long-term scientific survey of the Hessdalen phenomenon. *Journal of Scientitic Exploration*, 18:217–251, 06 2004.
- [57] U.S. Air Force. Unidentified Flying Objects and Air Force Project Blue Book, April 2003. URL <https://web.archive.org/web/20030624053806/http://www.af.mil/factsheets/factsheet.asp?fsID=188>. Accessed Jan 22, 2023.
- [58] U.S. Department of Defense. DoD Announces the Establishment of the All-domain Anomaly Resolution Office, July 20 2022. URL <https://www.defense.gov/News/Releases/Release/Article/3100053/>

dod-announces-the-establishment-of-the-all-domain-anomaly-resolution-office/. Accessed Jan 22, 2023.

- [59] U.S. Senate, 117th Congress, 2nd Session. Intelligence Authorization Act For Fiscal Year 2023, July 20 2022. URL <https://www.congress.gov/117/crpt/srpt132/CRPT-117srpt132.pdf#page=12>. Accessed Jan 22, 2023.
- [60] B. Villarroel and G. W. Marcy. Astronomical anomalies: Their role in the quest for extraterrestrial life, 2310.14895.
- [61] B. Villarroel, G. W. Marcy, S. Geier, A. Streblyanska, E. Solano, V. N. Andruk, M. E. Shultz, A. C. Gupta, and L. Mattsson. Exploring nine simultaneously occurring transients on April 12th 1950. *Scientific Reports*, 11(1), Jun 2021. doi: 10.1038/s41598-021-92162-7. URL <https://doi.org/10.1038/s41598-021-92162-7>.
- [62] B. Villarroel, E. Solano, H. Guergouri, A. Streblyanska, L. Mattsson, R. E. Bär, J. Mimouni, S. Geier, A. C. Gupta, V. Okororie, K. Laggoune, M. E. Shultz, R. A. F. Jr., and M. J. Ward. Is there a background population of high-albedo objects in geosynchronous orbits around earth?, 2204.06091.
- [63] G. Voorhis, J. Turner, S. Wood, A. Garcia, K. Knuth, C. Levy, M. Szydagis, C. Segar, R. Segar, B. Placek, R. Hoffman, and B. Kugielsky. UAPx, July 2021. URL <https://www.uapexpedition.org/>, <https://www.uapexpedition.org/team>, <https://www.uapexpedition.org/science>. Accessed 10-18-23.
- [64] W. A. Watters, A. Loeb, F. Laukien, R. Cloete, A. Delacroix, S. Dobroshinsky, B. Horvath, E. Kelderman, S. Little, E. Masson, A. Mead, M. Randall, F. Schultz, M. Szenher, F. Vervelidou, A. White, A. Ahlström, C. Cleland, S. Dockal, N. Donahue, M. Elowitz, C. Ezell, A. Gersznowicz, N. Gold, M. G. Hercz, E. Keto, K. H. Knuth, A. Lux, G. J. Melnick, A. Moro-Martín, J. Martin-Torres, D. L. Ribes, P. Sail, M. Teodorani, J. J. Tedesco, G. T. Tedesco, M. Tu, and M.-P. Zorzano. The Scientific Investigation of Unidentified Aerial Phenomena (UAP) Using Multimodal Ground-Based Observatories. *Journal of Astronomical Instrumentation*, 12(01), Mar. 2023. ISSN 2251-1725. URL <http://dx.doi.org/10.1142/S2251171723400068>.